Master's thesis

NTNU
Norwegian University of Science and Technology
Faculty of Information Technology and Electrical Engineering
Department of Mathematical Sciences

Petter Nøst

Optimal Control of Multibody Dynamics with Applications

Master's thesis in Applied Physics and Mathematics
Supervisor: Elena Celledoni
July 2023

NTNU
Norwegian University of
Science and Technology

Petter Nøst

Optimal Control of Multibody Dynamics with Applications

Master's thesis in Applied Physics and Mathematics
Supervisor: Elena Celledoni
July 2023

Norwegian University of Science and Technology
Faculty of Information Technology and Electrical Engineering
Department of Mathematical Sciences

NTNU
Norwegian University of
Science and Technology

Abstract

We present an approach for representing beams using multibody dynamics, specifically a system of rigid links known as a chain of pendulums. By introducing terms that penalize angles between subsequent pendulums, we add stiffness and rigidity to the system, making it suitable for simulating real-life beams and achieving desired trajectories or configurations through optimal control techniques. As applicable solvers have been shown to exhibit good long-term behavior, a variational approach is chosen. Theory of Hamiltonian systems is presented, and correct implementation and order of the numerical method is confirmed.

Furthermore, we explore a classical beam theory, known as the Euler-Bernoulli beam, where a derivation of the beam model is performed to show similarities to our model as the same angles are considered. Discretizing the Euler-Bernoulli beam equation and comparing it to our model, we observe comparable structural characteristics. Numerical experiments of the beam models in a Cantilever configuration reveal qualitative similarities, although concerns arise regarding the implementation of the free end of the Euler-Bernoulli model.

Expanding the Chain of Pendulums model, we account for different beam support configurations and incorporate dissipative forces such as drag. Through comparisons with the Euler-Bernoulli beam and static beam expressions, we demonstrate the feasibility of the Chain of Pendulums model for beam simulation.

As a representative application, we consider the marine riser system connected to a floating oil platform within the context of control theory. We investigate the impact of a control force applied at the oil platform and demonstrate the capability of the model to simulate the system. Specifically, we show that by applying a force at the oil platform, the bending moment at the seabed can be reduced. Through the utilization of optimal control, we determine the optimal control force using sequential least squares programming aided by a gradient-descent stepping algorithm when the applied control force remains constant. However, when the control force is considered variable, the control force-bending moment relationship is shown to become highly nonconvex, making it challenging to find global minima. Nonetheless, we identify minima that highlight the advantages of employing a variable force.

Sammendrag

Vi presenterer en metode for å representere bjelker ved hjelp av flerkroppsdynamikk, nærmere bestemt et system av stive ledd som kalles en pendelkjede. Ved å innføre ledd i uttrykket som straffer vinkler mellom påfølgende pendler legger vi til stivhet i systemet, noe som gjør det egnet for å simulere virkelige bjelker og oppnå ønskede baner eller konfigurasjoner gjennom optimal kontroll. Ettersom aktuelle løsningsmetoder har vist seg å gi god langtidsoppførsel, velger vi en variasjonell tilnærming. Teori for Hamiltonske systemer presenteres, og korrekt implementering og konvergensorden av den numeriske metoden bekreftes.

Videre utforsker vi en klassiske bjelketeori, kjent som Euler-Bernoulli-bjelken, der en utledning av bjelkemodellen utføres for å vise likheter med vår modell, der det vises at de samme vinklene blir tatt i betraktning. Ved å diskretisere Euler-Bernoulli-bjelkeligningen og sammenligne den med vår modell, observerer vi like strukturelle egenskaper. Numeriske eksperimenter av bjelkemodellene i en utkragerbjelke viser kvalitative likheter, selv om det mistenkes en feil i implementeringen av den frie enden i Euler-Bernoulli-modellen.

Ved å utvide pendelkjedemodellen tar vi hensyn til ulike konfigurasjoner av bjelkeoppheng og inkluderer dissipative krefter som luftmotstand. Gjennom sammenligninger med Euler-Bernoulli-bjelken samt statiske bjelkeuttrykk viser vi at pendelkjedemodellen er egnet til å simulere bjelker.

Som et representativ eksempel tar vi for oss et marint stigerørsystem koblet til en flytende oljeplattform i konteksten kontrollteori. Vi undersøker effekten av en kontrollkraft som påføres oljeplattformen og demonstrerer modellens evne til å simulere systemet. Spesifikt viser vi at ved å påføre en kraft på oljeplattformen kan bøyemomentet ved havbunnen reduseres. Ved hjelp av optimal kontroll finner vi den optimale kontrollkraften ved å bruke en sekvensiell minste kvadraters metode og gradient-basert stegalgoritme når den påførte kontrollkraften er konstant. Når kontrollkraften varierer, viser det seg imidlertid at forholdet mellom kontrollkraft og bøyemoment blir særdeles ikke-konveks, noe som gjør det utfordrende å finne globale minimum. Likevel oppnår vi minima som fremhever fordelene ved å bruke en variabel kraft.

Preface

This thesis concludes my five-year master's degree program in Applied Physics and Mathematics, specializing in Industrial Mathematics, at the Norwegian University of Science and Technology. It is completed in the spring of 2023.

The project has been supervised by professor Elena Celledoni, who has been of tremendous help. Her expertise and guidance has been invaluable, the quality of my work would not be the same without her. Through good discussions and sparring sessions, many an epiphany has been had.

I would also like to extend my deepest gratitude to my friends, girlfriend, and parents for always being there for me. Their unwavering support and companionship has gotten me through every challenging moment on this journey. Thank you all. We made it in the end.

Trondheim, July 2023

Petter Nøst

Table of Contents

List of Figures

List of Tables

Introduction

Systems consisting of beams or rigid rods exist all around us, from the charging wire for your phone, to the endoscope in the healthcare industry, from the load bearing beams in your house, to long stiff marine risers connected to the seafloor. Even though the applications are vastly different, the fundamental essence is the same, they are objects where one dimension, the length, is significantly larger than the other two.

In some applications, by applying a control to one end, the other end can be made to achieve desired configurations. One example of this is in the healthcare industry where endoscopes are used to investigate the inside of your body. Wires travelling inside the endoscope are pulled which bends the tip at the other end. Another application, which is the motivating example of this thesis, is the system of the marine riser. A marine riser system consists of pipes carrying oil and gas from a wellhead attached to the seabed, to an oil platform at the water surface. Over the past few years, there has been a growing focus on fatigue in the wellhead and marine riser, and it has been discovered that semi-submersible rigs can heavily impact the longevity of the wellhead [1], [2]. As failure of the system can be disastrous, methods calculating the lifetime are conservative. It would thus be advantageous to extend this lifetime by counteracting the effects on the wellhead.

A semi-submersible rig is a floating oil platform. These platforms are kept in place in different ways. Some are moored, essentially attached to the seabed by several anchors, while others are controlled by motors or propulsion units to counteract the motions of the water [3]. The fatigue of the wellhead has been found to be related to the bending moment in the marine riser [2]. As these platforms can be moved, it is of interest to explore the possibility of reducing this bending moment by moving the platforms at the surface, thus reducing the fatigue, and increasing the lifetime.

Generally, we want to construct a dynamical model of a beam, and control it by a force applied at one end. The aim is to be able to apply an optimal control to the system to obtain the necessary forces to achieve desired trajectories and configurations. There exists several beam models that might be used for this purpose, however, they can be quite intricate and are not always easily comprehensible. We want two properties of our model. First, we want the terms to be simple, for the optimization, and understandable. Secondly, we want to consider models obtained through variational calculus as they are easy to discretize in a natural way with structure preserving time as well as space-time numerical methods. These integrators have shown good qualitative behavior, as well as a more precise long-term integration, compared to general-purpose methods [4].

To model a beam or a rigid rod as a multibody system consisting of a series of elements that are penalized when the angles between subsequent elements differ is not a novel idea, see for instance [5], [6]. In fact it is done when deriving one of the fundamental equations for long, thin beams, the Euler-Bernoulli beam theory [5]. However, instead of using the theory to derive such an equation, we are interested to know if a series of pendulums, with angles penalized by a spring term, can be a workable model for beam dynamics especially in the applications we have in mind. We compare this simple, but nonlinear model to the linear Euler-Bernoulli beam model in problems of optimal control inspired by offshore simulations.

The structure of this thesis is as follows. Chapter 1 introduces necessary theory of variational calculus and Hamiltonian systems, before numerical methods for solving such systems are presented. In Chapter 2, the beam models are examined. The Euler-Bernoulli beam is presented as a reference model, and a derivation of the model is done to show similarities to our model. Following that, the Chain of Pendulums model is introduced, and the models are compared analytically and

numerically. To account for different beam supports, our model is extended and compared to the Euler-Bernoulli beam in the Cantilever, Fixed-Fixed, and Pinned-Pinned configurations. As we desire a realistic model that is applicable to the industry, the model is further expanded to account for dissipation by the addition of a drag force. In Chapter 3 control is considered. First, a simple control force is applied to the system, and its effects on the system are investigated, where reduction of the bending moment at the wellhead of the marine riser system is used as the representative example. Then, to explore the possibilities of using our model to obtain optimal solutions of the control force, an optimal control method is considered. Finally, Chapter 4 recounts the results and concludes the thesis.

Chapter 1

Hamiltonian Systems

Mechanical systems can be modelled in different ways. While Newtonian mechanics is the basis of classical physics, there exists a formulation that is often more convenient. The Lagrangian is a scalar function of the kinetic and potential energy of a system. These terms are often easily found, making the construction of the Lagrangian rather simple. From the expression of the Lagrangian, governing equations of motion of the system can either be derived directly, or the Lagrangian can be transformed to the Hamiltonian. The Hamiltonian is, like the Lagrangian, also a scalar function of the energies. In a lot of cases it is even the total energy of the system. With the Hamiltonian, Hamilton's equations of motion can be derived. As Hamiltonian mechanics is widely used in the literature, numerical integrators with important qualitative properties of Hamiltonian equations, such as symplecticity, have been developed for systems in this form [4]. The structure of Sections 1.1-1.3 and the first half of Section 1.4 follows work done in my specialization project written in the fall of 2022, consisting of theory found in [4] and [7].

1.1 Configurations

To derive the Hamiltonian of a system, it is first necessary to establish a framework for describing mechanical systems. This is done by introducing the concept of *configurations* [7]. A configuration is a set of coordinates, denoted $q = \begin{bmatrix} q_1 & \dots & q_n \end{bmatrix}$, that uniquely determines the position and orientation of the system. In Euclidean space this could be represented by the x, y, z-coordinates, or any combination of variables that capture the characteristics of the system. In other words, a single mechanical system can have multiple descriptions based on the chosen coordinates. However, as configurations uniquely define the position and orientation it is also considered *minimal*, as no fewer variables can fully describe the system. The number of variables, n, corresponds to the degrees of freedom of the system [7]. The entire set of configurations forms the *configuration space*, which is often denoted Q. Thus, a configuration $q \in Q$ can be considered the coordinates of the configuration space.

To consider how mechanical systems evolve over time, we let $q(t) \in Q$ be the configuration at time t. Then the function $q : \mathbb{R} \to Q$ is the curve that describes the motion of the system starting in $q(0) = q_0$. If the components of $q = \begin{bmatrix} q_1 & \dots & q_n \end{bmatrix}$ are all continuously differentiable in time, the derivative of q is denoted as $\dot{q} = \begin{bmatrix} \dot{q}_1 & \dots & \dot{q}_n \end{bmatrix}$.

1.2 Equations of Motion

With this notation, we are now able to derive the equations of motion for the system. These equations describe how the system evolves in time, and we derive them using Hamilton's principle. To do this, it is first necessary to define some concepts. The Lagrangian is a real-valued function, and is typically defined as

$$L(q, \dot{q}) = K(q, \dot{q}) - V(q)$$

for mechanical systems, where $K(q, \dot{q})$ represents the kinetic energy and $V(q)$ the potential energy. As Hamilton's principle is a variational principle, we next need to introduce the variation of the

trajectory. Consider again the curve $q(t)$, with fixed endpoints $q(a) = q_a$ and $q(b) = q_b$. The variation of this trajectory is a smooth mapping [7]

$$(t, \epsilon) \mapsto q(t, \epsilon), \qquad a \leq t \leq b, \qquad \epsilon \in (-\delta, \delta) \subset \mathbb{R},$$

where $q(t, 0) = q(t)$ represents the true trajectory with no displacement, that still satisfies the fixed endpoints $q(a, \epsilon) = q_a$ and $q(b, \epsilon) = q_b$. The virtual displacement [7] is then defined as

$$\delta q(t) := \frac{\partial}{\partial \epsilon} q(t, \epsilon)|_{\epsilon=0}.$$

With these definitions in place, we can now state Hamilton's principle [7].

Definition 1. *Hamilton's principle. Let $q(t) \in Q$ be the configuration curve of a mechanical system in the interval $[a, b]$ with fixed endpoints at $q(a) = q_a$ and $q(b) = q_b$. The Lagrangian of the system is $L(q, \dot{q})$, and $\delta q(t)$ is any displacement. If and only if this curve satisfies*

$$\delta \int_a^b L(q(t), \dot{q}(t))dt = 0,$$

it represents a correct evolution of the system.

With this definition, the equations of motion can be derived as follows. We start by taking variations,

$$\frac{d}{d\epsilon} \int_a^b L(q(t, \epsilon), \dot{q}(t, \epsilon))dt|_{\epsilon=0} = 0$$
$$\int_a^b \left(\frac{\partial L}{\partial q} \delta q + \frac{\partial L}{\partial \dot{q}} \delta \dot{q} \right) dt = 0.$$

By now isolating the second term and considering that $\delta \dot{q} = \frac{d}{dt} \delta q$, we can integrate by parts to get

$$\int_a^b \frac{\partial L}{\partial \dot{q}} \frac{d}{dt} \delta q dt = \frac{\partial L}{\partial \dot{q}} \delta q \Big|_a^b - \int_a^b \frac{d}{dt} \frac{\partial L}{\partial \dot{q}} \delta q dt = - \int_a^b \frac{d}{dt} \frac{\partial L}{\partial \dot{q}} \delta q dt,$$

where the final equality is a result of the displacement being zero at the boundary points. Hamilton's principle can then be restated as

$$\int_a^b \left(-\frac{d}{dt} \frac{\partial L}{\partial \dot{q}} + \frac{\partial L}{\partial q} \right) \delta q dt = 0.$$

This holds for any displacement $\delta q(t)$, and we arrive at the equations of motion, known as the Euler-Lagrange equations,

$$\frac{d}{dt} \frac{\partial L}{\partial \dot{q}} - \frac{\partial L}{\partial q} = 0. \tag{1.2.1}$$

These equations describe how the system that is defined by the Lagrangian $L(q, \dot{q})$ evolves in time.

By considering a transformation, this system can be simplified further. If the Hessian matrix $\frac{\partial^2 L}{\partial \dot{q}^2}$ of the Lagrangian is non-singular, the Lagrangian is considered regular. With a regular Lagrangian one can perform a change of variables known as the Legendre transformation [7]. Let p represent the *conjugate momentum* that is given as $p = \frac{\partial L}{\partial \dot{q}}$. By now considering the change of variables from $(q, \dot{q})$ to (q, p), the Hamiltonian is defined as

$$H(q, p) = p^T \dot{q} - L(q, \dot{q}). \tag{1.2.2}$$

The equivalent of the Euler-Lagrange equations can now be derived by differentiating the Hamiltonian and considering $\dot{q} = \dot{q}(q, p)$ as a function of q and p,

$$\frac{\partial H}{\partial p} = \dot{q} + \left(\frac{\partial \dot{q}}{\partial p} \right)^T p - \left(\frac{\partial \dot{q}}{\partial p} \right)^T \frac{\partial L}{\partial \dot{q}} = \dot{q}$$
$$\frac{\partial H}{\partial q} = \left(\frac{\partial \dot{q}}{\partial q} \right)^T p - \frac{\partial L}{\partial q} - \left(\frac{\partial \dot{q}}{\partial q} \right)^T \frac{\partial L}{\partial \dot{q}} = -\frac{\partial L}{\partial q} = -\frac{d}{dt} \frac{\partial L}{\partial \dot{q}} = -\dot{p}.$$

This gives us Hamilton's equations of motion

$$\dot{q} = \frac{\partial H}{\partial p}, \qquad \dot{p} = -\frac{\partial H}{\partial q}, \tag{1.2.3}$$

which can be rewritten on matrix form as

$$\begin{bmatrix} \dot{q} \\ \dot{p} \end{bmatrix} = \begin{bmatrix} 0 & I_n \\ -I_n & 0 \end{bmatrix} \nabla H(q,p) = J \nabla H(q,p). \tag{1.2.4}$$

An important trait of the Hamiltonian comes from considering the kinetic energy. The kinetic energy term in the Lagrangian is often on the form $K(q,\dot{q}) = \frac{1}{2}\dot{q}^T M(q)\dot{q}$. If the Lagrangian is regular, and the mass matrix $M(q)$ is symmetric positive definite, the momentum becomes $p = M(q)\dot{q}$, equivalently, $\dot{q} = M(q)^{-1}p$. Inserting this into the Hamiltonian, this results in

$$\begin{aligned} H(q,p) &= p^T M(q)^{-1} p - L(q, M(q)^{-1}p) = p^T M(q)^{-1} p - \frac{1}{2} p^T M(q)^{-1} p + V(q) \\ &= \frac{1}{2} p^T M(q)^{-1} p + V(q) = K(q, M(q)^{-1}p) + V(q). \end{aligned}$$

In other words, the Hamiltonian of a regular Lagrangian is the total energy [7].

1.3 Properties of Unconstrained Systems

As it is necessary to implement constraints in our model, theory concerning constrained Hamiltonian systems will be presented. However, first some properties of unconstrained systems are considered.

Energy preservation. Through the use of the definitions of the Hamilton's equations (1.2.3), differentiating the Hamiltonian gives a nice result

$$\frac{d}{dt} H(q,p) = \frac{\partial H}{\partial q}\dot{q} + \frac{\partial H}{\partial p}\dot{p} = \frac{\partial H}{\partial q}\frac{\partial H}{\partial p} + \frac{\partial H}{\partial q}\left(-\frac{\partial H}{\partial q}\right) = 0.$$

In other words, the Hamiltonian is constant. If we further consider the Hamiltonian as a function of $(q,\dot{q})$ we can write

$$E(q,\dot{q}) = H(q, p(q,\dot{q})) = \dot{q}^T \frac{\partial L}{\partial \dot{q}}(q,\dot{q}),$$

showing that for certain systems previously described, the energy is preserved. Further, if we consider the Euler-Lagrange equations this can be shown even when the Lagrangian is not regular [7],

$$\begin{aligned} \frac{d}{dt} E(q,\dot{q}) &= \frac{d}{dt}\left(\dot{q}^T \frac{\partial L}{\partial \dot{q}} - L\right) = \ddot{q}^T \frac{\partial L}{\partial \dot{q}} + \dot{q}^T \frac{d}{dt}\frac{\partial L}{\partial \dot{q}} - \ddot{q}^T \frac{\partial L}{\partial \dot{q}} - \dot{q}^T \frac{\partial L}{\partial q} \\ &= \dot{q}^T \left(\frac{d}{dt}\frac{\partial L}{\partial \dot{q}} - \frac{\partial L}{\partial \dot{q}}\right) = 0, \end{aligned}$$

where the Euler-Lagrange equations give the final equality.

Reversibility. To consider the reversibility of a system, divide the variables into two groups, $y = (u,v)$. Then consider a map ϕ_t that takes an initial condition $y(0) = (u(0), v(0))$ and associates it with the solution at time t, $y(t) = (u(t), v(t))$, represented as $\phi_t(y(0)) = y(t)$. Now by considering an even mapping $\rho(u,v) = (u,-v)$, the flow of the system is reversible if it satisfies [4]

$$\phi_t \circ \rho \circ \phi_t = \rho.$$

A system with a reversible flow is also called symmetric. Thus, if a Hamiltonian is even, $H(q,p) = H(q,-p)$, the flow of the Hamiltonian equations is reversible, and symmetric [4].

Symplecticity. Let $I \in \mathbb{R}^n$, $U \subset \mathbb{R}^{2n}$, and define the skew-symmetric matrix

$$J = \begin{bmatrix} 0 & I \\ -I & 0 \end{bmatrix}.$$

A differential map $g : U \to \mathbb{R}^{2n}$ is symplectic if the Jacobian matrix $g'(q,p)$ satisfies the condition [4]

$$g'(q,p)^T J g'(q,p) = J.$$

The flow of the Hamiltonian equations is symplectic [4].

1.4 Constrained Mechanical Systems

A constraint is a property added to the system that restricts its possible evolution or configurations. These constraints can be expressed by algebraic equations in the configuration and velocity variables. If the constraint equations are of the form

$$b(q) = 0,$$

or can be integrated to obtain this form, such as

$$\sum_{i=1}^{n} \frac{\partial b}{\partial q_i}\dot{q}_i = 0,$$

the constraints are called holonomic. Otherwise, they are called non-holonomic constraints [7]. In this thesis will consider only holonomic constraint. These constraints involve only the configuration variables.

With holonomic constraints, it can be shown that the Euler-Lagrange equations can be rewritten [8]

$$\begin{aligned} \frac{d}{dt}\frac{\partial L}{\partial \dot{q}} - \frac{\partial L}{\partial q} + G(q)^T\lambda &= 0 \\ g(q) &= 0, \end{aligned}$$

where $G(q) = \frac{dg}{dq}(q)$ is the Jacobian of the constraints $g(q) = 0$ and $\lambda = \begin{bmatrix}\lambda_1 & \dots & \lambda_m\end{bmatrix}^T$ is a vector of Lagrange multipliers. An approach to obtain this is to consider the altered Lagrangian [8]

$$L^\alpha(q, \dot{q}, \lambda) = L(q, \dot{q}) - g(q)^T\lambda,$$

which leas to the desired equations.

As with the non-constrained system, if the considered Lagrangian is regular, we can apply the Legendre transformation and obtain

$$p = \frac{\partial L^\alpha(q, \dot{q}, \lambda)}{\partial \dot{q}},$$

giving the altered Hamiltonian

$$H^\alpha(q, p, \lambda) = p^T\dot{q} - L^\alpha(q, \dot{q}, \lambda) = p^T\dot{q} - L(q, \dot{q}) + g(q)^T\lambda = H(q, p) + g(q)^T\lambda.$$

Then Hamilton's equations are given as

$$\begin{aligned} \frac{\partial H^\alpha}{\partial p} &= \frac{\partial H}{\partial p} = \dot{q}, \\ \frac{\partial H^\alpha}{\partial q} &= \frac{\partial H}{\partial q} + G(q)^T\lambda = -\frac{\partial L}{\partial q} + G(q)^T\lambda = -\frac{d}{dt}\frac{\partial L}{\partial \dot{q}} = -\dot{p}, \end{aligned}$$

resulting in the equations of motion

$$\begin{aligned} \dot{q} &= \frac{\partial H}{\partial p} \\ \dot{p} &= -\frac{\partial H}{\partial q} - G(q)^T\lambda, \end{aligned}$$

with constraints $g(q) = 0$. Equivalently in matrix formulation

$$\begin{aligned} \begin{bmatrix}\dot{q} \\ \dot{p}\end{bmatrix} &= J\nabla H(q, p) - \begin{bmatrix}0 \\ G(q)^T\lambda\end{bmatrix} \\ g(q) &= 0, \end{aligned}$$

where J is the skew-symmetric matrix as before.

1.5 Properties of Holonomically Constrained Systems

Now the same properties are considered if they are preserved with constraitns.

Energy Preservation. Again if we define the Hamiltonian as $H(q, p(q, \dot{q}))$, the energy becomes

$$E(q, \dot{q}) = H(q, p(q, \dot{q})) = \dot{q}^T \frac{\partial L}{\partial \dot{q}}(q, \dot{q}) - L(q, \dot{q}).$$

We can then consider the time derivative of the energy of the constrained system

$$\begin{aligned}\frac{d}{dt}E(q, \dot{q}) &= \frac{d}{dt}\left(\dot{q}^T \frac{\partial L}{\partial \dot{q}} - L\right) = \ddot{q}^T \frac{\partial L}{\partial \dot{q}} + \dot{q}^T \frac{d}{dt}\frac{\partial L}{\partial \dot{q}} - \ddot{q}^T \frac{\partial L}{\partial \dot{q}} - \dot{q}^T \frac{\partial L}{\partial q} \\ &= \dot{q}^T \left(\frac{d}{dt}\frac{\partial L}{\partial \dot{q}} - \frac{\partial L}{\partial q}\right) = \dot{q}^T G(q)^T \lambda = 0,\end{aligned}$$

where the final equality comes from differentiating the constraint with regards to time

$$0 = \frac{dg}{dt}(q) = G(q)\dot{q},$$

showing that the energy is conserved [4].

Reversibility. As with the unconstrained system, if the Hamiltonian is even, $H(q, p) = H(q, -p)$, the system is reversible [4, p. 240].

Symplecticity. It is shown in [4, p. 241] that the flow of the system is symplectic as long as $H(q, p)$ and $g(q)$ are twice continuously differentiable.

1.6 Numerical Integrators

As Hamiltonians possess the properties previously described, numerical methods have been developed to conserve them. Theory of the following two methods can be found in [4]. The conservation of these properties results in an improved qualitative behavior, as well as a more precise long-term integration, compared to general-purpose methods. As Hamiltonian systems with holonomic constraints have been shown to be symmetric and symplectic, it is desirable to use integrators that are both symmetric and symplectic. Symplectic integrators preserve the symplecticity that the Hamiltonian exhibits, while symmetric integrators preserve the reversibility.

One method proposed for separable Hamiltonians of the structure

$$\begin{aligned}H(q, p) &= \frac{1}{2}p^T M^{-1} p + U(q) \\ g(q) &= 0\end{aligned}$$

with constant mass matrix M, is the SHAKE method, which is constructed as follows

SHAKE.

$$\begin{aligned}q_{n+1} - 2q_n + q_{n-1} &= -h^2 M^{-1}\left(U_q(q_n) + G(q_n)^T \lambda_n\right) \\ 0 &= g(q_{n+1}).\end{aligned}$$

The momentum p is not used in the method and is approximated by $p_n = M(q_{n+1} - q_{n-1})/2h$. The three-term recursion may accumulate round-off errors, making the reformulation as a one-step method desirable. To address this, an alternative method was developed.

RATTLE.

$$\begin{aligned}p_{n+1/2} &= p_n - \frac{h}{2}\left(U_q(q_n) + G(q_n)^T \lambda_n\right) \\ q_{n+1} &= q_n + hM^{-1} p_{n+1/2} \\ 0 &= g(q_{n+1}) \\ p_{n+1} &= p_{n+1/2} - \frac{h}{2}\left(U_q(q_{n+1} + G(q_{n+1})^T \lambda_{n+1}\right).\end{aligned}$$

However, the Lagrange multiplier λ_{n+1} is not available yet, as it is computed in the step with q_{n+2}. To remedy this, it was proposed to replace the final equation with a projection step as

$$\begin{aligned} p_{n+1} &= p_{n+1/2} - \frac{h}{2}\left(U_q(q_{n+1} + G(q_{n+1})^T \mu_n\right) \\ 0 &= G(q_{n+1}) M^{-1} p_{n+1}. \end{aligned}$$

Another advantage of this method is that it projects p_{n+1} on the manifold, causing the solution (q_{n+1}, p_{n+1}) to also lie on the solution manifold. This method has further been extended to general Hamiltonians as

$$\begin{aligned} p_{n+1/2} &= p_n - \frac{h}{2}\left(H_q(q_n, p_{n+1/2}) + G(q_n)^T \lambda_n\right) \\ q_{n+1} &= q_n + \frac{h}{2}\left(H_p(q_n, p_{n+1/2}) + H_p(q_{n+1}, p_{n+1/2})\right) \\ 0 &= g(q_{n+1}) \\ p_{n+1} &= p_{n+1/2} - \frac{h}{2}\left(H_q(q_{n+1}, p_{n+1/2}) + G(q_{n+1})^T \mu_n\right) \\ 0 &= G(q_{n+1}) H_p(q_{n+1}, p_{n+1}). \end{aligned} \tag{1.6.1}$$

The three first equations determine $(q_{n+1}, p_{n+1/2}, \lambda_n)$ and the last two determine (p_{n+1}, μ_n). This method is symmetric, symplectic, and convergent of order two [4].

Chapter 2

Beam Models

A beam is characterized as a slender structure where one dimension is significantly larger than the other two. The axis of the beam is aligned with the longer dimension, and the cross-section perpendicular to this axis is assumed to smoothly vary along the length of the beam. The solid mechanics theory of beams, or beam theory, is an important part in structural analysis as it is a simple tool that lets designers analyze various structures. While more advanced techniques like the finite element method are now widely available for stress analysis of complex structures, beam models are frequently used during the design phase, as they offer a continuous model and valuable insight on the structural behavior and has proven useful in validating computational solutions [9].

When it comes to beam theories, several have been formulated, each relying on different assumptions, resulting in varying degrees of accuracy and application. Among these theories, one of the simplest and most useful was proposed by Euler and Bernoulli, commonly known as the Euler-Bernoulli beam theory [9]. This is widely used in the industry, and can be used to describe many different mechanical flexible systems [10]. Specifically, in the literature it is a common model in use for marine risers [2], [11], [12]. This, along with some similarities that will be shown, is why the Euler-Bernoulli beam is a natural choice of reference for comparison to our model.

The focus of this thesis revolves around a model derived from a chain of pendulums. Our aim is to investigate the potential application of this chain of pendulums system as a beam model. To achieve this, we introduce torsional springs between the pendulums to constrain their dynamics and apply rigidity to the system. This approach falls under the domain of multibody dynamics, as the chain of pendulums represents a series of interconnected elements. The concept of multibody dynamics as a means to model beam systems is common in the literature [13], [14], [15], [16].

One compelling reason for considering this approach is that it can be formulated as a variational problem, exhibiting favorable properties outlined in Section 1.5. Moreover, there exist methods, Section 1.6, that preserve these properties, ensuring good long-term behavior. Since our focus lies in modeling real-life systems, such characteristics are desirable. Furthermore, the chain of pendulums is a known concept, making the beam model easily comprehensible, and provides a solid foundation that can be further improved upon to achieve desired properties that reflect real-life systems. This is done by introducing or modifying terms in the Hamiltonian, constraints, or equations of motion.

2.1 Euler-Bernoulli Beam Theory

The Euler-Bernoulli beam model is considered one of the classical beam theories. The theory is utilized in analysis of long, thin beams. In cases of shorter beams, considerations of torsion and shear deformation become necessary. However, in beams with a length-to-thickness ratio exceeding approximately 10 to 20, these effects can be disregarded [17]. The present theory mostly follows [9].

The Euler-Bernoulli Beam Theory makes three assumptions:

1. Infinitely Rigid Cross-Section: The cross-section is undeformable in its own plane.
2. Planar Cross-Section: The cross-section remains plane after deformation.

3. Normality to Deformed Axis: The cross-section remains normal to the deformed axis of the beam.

Consider a coordinate system (x, y, z) placed in the cross-section of the beam, where the xz-plane represents the cross-section and the y-axis is aligned with the axis of the beam. Let $u_x(x, y, z)$, $u_y(x, y, z)$, and $u_z(x, y, z)$ denote the displacements of a point along the respective axes.

The first assumption states that the cross-section of a beam is undeformable in its own plane. This implies that the displacement in the cross-sectional plane can be represented by two rigid body translations, $\bar{u}_x(y)$ and $\bar{u}_z(y)$, independent of x and z [9],

$$u_x(x, y, z) = \bar{u}_x(y) \quad u_z(x, y, z) = \bar{u}_z(y).$$

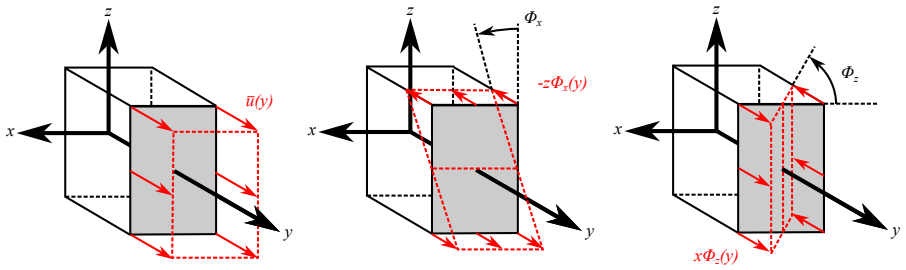

Figure 2.1: Decomposition of the axial displacement of a beam.

The second assumption states that the cross-section of the beam remains plane after deformation. This means that the axial displacement consists of a rigid body translation $\bar{u}_y(y)$ and two rigid body rotations $\Phi_x(y)$ and $\Phi_z(y)$ [9]. This is illustrated in Figure 2.1. The axial displacement can be expressed as

$$u_y(x, y, z) = \bar{u}_y(y) + x\Phi_z(y) - z\Phi_x(y).$$

It is desirable to write the rigid body translations of the cross-section $\bar{u}_x(y)$, $\bar{u}_y(y)$, and $\bar{u}_z(y)$, as positive in the directions of (x, y, z), hence the sign convention as seen in Figure 2.1.

The third assumption states that the cross-section remains normal to the deformed axis of the beam. This means that the slope of the beam and the rotation of the section is equal [9],

$$\Phi_x = \frac{d\bar{u}_z}{dy}(y) \quad \Phi_z = -\frac{d\bar{u}_x}{dy}(y).$$

This is shown in Figure 2.2, which also explains the negative term in the second equation.

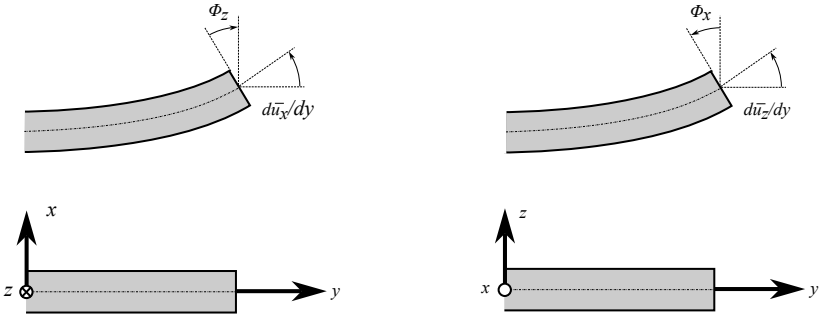

Figure 2.2: Slope and rotation of cross-section.

These assumptions lead to the following displacement field for the Euler-Bernoulli beam,

$$\begin{aligned} u_x(x, y, z) &= \bar{u}_x(y) \\ u_y(x, y, z) &= \bar{u}_y(y) - x\frac{d\bar{u}_x}{dy}(y) - z\frac{d\bar{u}_z}{dy}(y) \\ u_z(x, u, z) &= \bar{u}_z(y). \end{aligned}$$

Notice that the three-dimensional displacement field is now defined in terms of three displacements $\bar{u}_x(x)$, $\bar{u}_y(x)$, and $\bar{u}_z(x)$, and their derivatives with regards to y. This simplification is a result from the assumptions, and allow the further development of a one-dimensional beam theory, a theory where the displacements are functions purely of the axial coordinate, y.

It is assumed that a beam under purely axial load only experiences axial displacement, i.e. $u_y(x, y, z) = \bar{u}_y(y)$. Further, transverse loads are assumed to only cause transverse displacement and curvature of the beam [9]. In a beam of constant cross-section, the yz-plane is a plane of symmetry. If the loads considered are only applied in this plane, the resulting displacement is also confined to this plane. Hence, the displacement field for a beam under transverse load simplifies to

$$\begin{aligned} u_x(x, y, z) &= 0 \\ u_y(x, y, z) &= -z\frac{d\bar{u}_z}{dy}(y) \\ u_z(x, u, z) &= \bar{u}_z(y) \end{aligned}$$

For beams subjected to transverse loads, the displacement of interest is often in the same direction as the applied loads, typically the vertical direction with respect to gravity. The third assumption raises a point regarding the size of the admissable deflections. As the beam undergoes larger displacements, transverse shear forces become significant, causing the cross-section to not be normal to the deformed axis of the beam. As this is not something the Euler-Bernoulli model is designed to take into account, the theory only applies to small displacements in long, thin beams [17]. Therefore, when assuming sufficiently small displacements, the displacement angles $\theta = \frac{d\bar{u}_z}{dy}(y)$ are small, resulting in neglible displacement in the axial direction y. In fact, literature often states that the Euler-Bernoulli beam theory assumes no axial deformation [17]. Consequently, the displacement considered for a beam under transverse load often only involves the z-direction, $u_z(x, y, z) = \bar{u}_z(y)$. Notice now that we are considering the z displacement in the yz-plane, showing that the deflection can be expressed purely as a function of y

$$z = z(y).$$

2.1.1 Derivation of the Euler-Bernoulli Beam Equation

The Euler-Bernoulli equation can be derived using different approaches. One approach involves considering moments, shear force, and curvature, as described in [9] and [17]. The approach we follow, which illustrates similarities to our Chain of Pendulums model, involves discretizing the beam and employing finite difference, as done in [5].

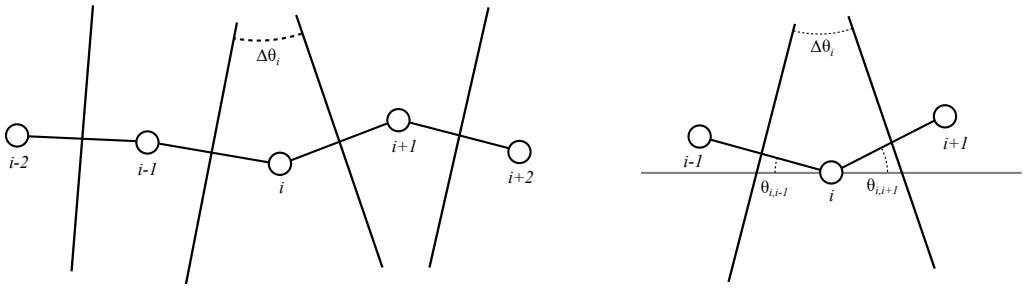

Figure 2.3: Left: A beam as a series of slabs with defining angle $\Delta\theta_i$. Right: Definition of the defining angle $\Delta\theta_i$.

Consider the beam as a series of slabs, with each slab corresponding to a node, as shown in Figure 2.3(left). When there is a difference between the two angles of a slab we suppose that the potential energy of the slab increases as it desires to return to its neutral position of zero energy. Let the difference of angles in a slab be denoted $\Delta\theta_i$. We then obtain the total energy of the slabs from Hooke's law as [5]

$$U = \frac{1}{2}\frac{C}{d}\sum_{i=2}^{n-1}(\Delta\theta_i)^2\,, \tag{2.1.1}$$

where C is the stiffness parameter, and d the y-, or horizontal, component of the discretized elements. The angles are considered positive when measured from the horizontal axis to the element. For instance, in the case of Figure 2.3(right), $\theta_{i,i-1}$ would be negative. Note for later that this angle difference is equivalent to the angle we will consider in the Chain of Pendulums model.

Now, consider the angle between node i and node $i+1$, which is denoted $\theta_{i,i+1}$. Due to the assumption of small deflections, we can make use of two approximations, the small angle approximation $\tan(\theta) \approx \theta$, and that the y-component, d, is approximately equal to the length of the element. The difference in angles can then be approximated [5]

$$\Delta\theta_i = \theta_{i,i+1} - \theta_{i-1,i} \approx \frac{z_{i+1} - z_i}{d} - \frac{z_i - z_{i-1}}{d} = \frac{z_{i+1} - 2z_i + z_{i-1}}{d}.$$

Notice that this is equivalent to the finite central difference approximation of the second derivative, except for a missing a factor $1/d$. By substituting this approximation into equation (2.1.1) we obtain

$$U = \frac{1}{2}\frac{C}{d^3}\sum_{i=2}^{n-1}(2z_i - z_{i+1} - z_{i-1})^2. \tag{2.1.2}$$

Furthermore, we can consider the z-component of the internal force acting on node i by differentiating with respect to z_i

$$f_i^z = -\frac{\partial U}{\partial z_i} = \frac{C}{d^3}[z_{i-2} - 4z_{i-1} + 6z_i - 4z_{i+1} + z_{i+2}].$$

This expression corresponds to the finite central difference approximation of the fourth derivative, except for a missing factor $-1/d$. This leads to

$$f(y) \approx -Cd\frac{d^4z}{dy^4}.$$

As work is the product of force applied times distance traveled, we can consider the work done to a slab by an external force as $W_i = F_i z_i$. To implement this, we include the work in the potential energy (2.1.2) with a negative sign to align with convention [5]

$$U = \frac{1}{2}\frac{C}{d^3}\sum_{i=2}^{n-1}(2z_i - z_{i+1} - z_{i-1})^2 - F_i z_i. \tag{2.1.3}$$

The total force is then given as

$$f(y) \approx -Cd\frac{d^4z}{dy^4} + F(y).$$

Thus, by applying Newton's second law, we get the dynamic equation

$$m\frac{dz^2}{dt^2} = -Cd\frac{d^4z}{dy^4} + F(y),$$

where m represents the mass and $F(y)$ is the external force. The corresponding static equation can be derived as

$$C\frac{d^4z}{dy^4} = F/d = w(y), \tag{2.1.4}$$

where $w(y)$ is the load per unit length. It can be shown that the parameter C is equal to Young's modulus, E, times the area moment of inertia, I [5]. This is known as the flexural rigidity of the beam. Thus, we arrive at the dynamic Euler-Bernoulli equation

$$\mu\frac{d^2z}{dt^2} = -EI\frac{d^4z}{dy^4} + w(y), \tag{2.1.5}$$

where μ is the mass per unit length.

2.2 The Chain of Pendulums Model

The beam model we are considering is derived from the concept of a chain of pendulums. The theory of a chain of pendulums without springs can be found in [8], which we use as our basis. A chain of pendulums consists of a series of rigid links connected by spherical joints. The links are considered massless, with all the mass concentrated in the end of each link. To introduce stiffness and simulate the behavior of a beam, torsional springs are attached between successive pendulums. These springs serve to restrain the movement of the pendulums and provide rigidity to the system. The first pendulum in the chain is connected to a fixed base through a spherical joint, and a spring is incorporated to provide boundary stiffness. The system is initially considered in a gravitational field, before the force is later generalized.

An important consideration is the choice of coordinate system to represent the chain. While using spherical coordinates might seem natural, since we are interested in the angles between pairs of pendulums, the compexity of the kinetic energy term has been found to increase significantly as the number of pendulums grows. Instead, we define the coordinates of the nodes using cartesian coordinates.

As we intend to apply this model to long, thin, rigid beams, we assume that axial deformation is considerably smaller than transverse deformation and neglect it. To ensure this, we impose the constraint that the lengths of the pendulums remain constant.

A preliminary result of the single spherical pendulum is first presented, before the system of a chain is considered.

2.2.1 Spherical Pendulum

Let $q = \begin{bmatrix} x & y & z \end{bmatrix} \in S^2$ be the attitude vector of the pendulum, where S^2 represents the unit sphere. The mass of the pendulum is denoted m, and the length l. The speed of the mass is then given as $l\dot{q}$, which yields the kinetic energy of the spherical pendulum [8]

$$K(\dot{q}) = \frac{1}{2} m l^2 \|\dot{q}\|^2.$$

The potential energy of the simple spherical pendulum given in [8] consists only of gravity. The gravitational energy is defined by the the z-coordinate of the mass. As the pendulum resides on the unit sphere S^2, where the z-component ranges from -1 to 1, the gravitational term is formulated to attain maximum energy at the peak, where $q = \begin{bmatrix} 0 & 0 & 1 \end{bmatrix}$. This results in the gravitational energy

$$E^G(q) = mgl(e_3^T q + 1),$$

where $e_3^T = \begin{bmatrix} 0 & 0 & 1 \end{bmatrix}$ is the standard unit vector.

As we later want to consider rigid beams, we need to add stiffness to the system. This is done by introducing torsional springs. In addition to the spherical joint connecting the pendulum to the fixed base, a spring is attached between the pendulum and a constant initial vector, q_0. The spring restrains the movement of the pendulum when it moves away from the initial vector. To express the angle θ between the pendulum and the vector, we consider the scalar product

$$q_0^T q = \|q_0\| \|q\| \cos(\theta),$$

yielding the expression for the angle between the vectors as

$$\theta = \arccos\left(\frac{q_0^T q}{\|q_0\| \|q\|} \right) = \arccos\left(q_0^T q \right),$$

where the final equality comes from the lengths of both vectors being 1.

By applying Hooke's law for the elastic energy of a torsional spring with spring constant k,the elastic energy term is given by

$$E^E(q) = \frac{1}{2} k \theta^2 = k \arccos^2(q_0^T q).$$

Together with the gravitational energy, this defines the total potential energy

$$U(q) = mgl(e_3^T q + 1) + k \arccos^2(q_0^T q).$$

Combining the kinetic and potential energy, the Lagrangian for the spherical pendulum restrained by a spring in a gravitational field is

$$L(q, \dot{q}) = \frac{1}{2} ml^2 \|\dot{q}\|^2 - mgl(e_3^T q + 1) - k \arccos^2(q_0^T q).$$

As we are concerned with long, thin, rigid beams, we introduce a constraint on the length of the pendulum to restrict the movement in the axial direction

$$g(q) = \frac{1}{2}(\|q\|^2 - 1) = 0,$$

which implies that the attitude vector q must always be of unit length. The associated Jacobian is denoted $G(q) = \frac{dg}{dq} = q^T$.

To obtain the Hamiltonian of the system, we perform the Legendre transformation to get the conjugate momentum

$$p = \frac{\partial L}{\partial \dot{q}} = ml^2 \dot{q} \implies \dot{q} = \frac{1}{ml^2} p.$$

The Hamiltonian of the spherical pendulum restrained by a spring in a gravitational field is then

$$H(q, p) = \frac{1}{2ml^2} \|p\|^2 + mgl(e_3^T q + 1) + k \arccos^2(q_0^T q).$$

2.2.2 Chain of Pendulums

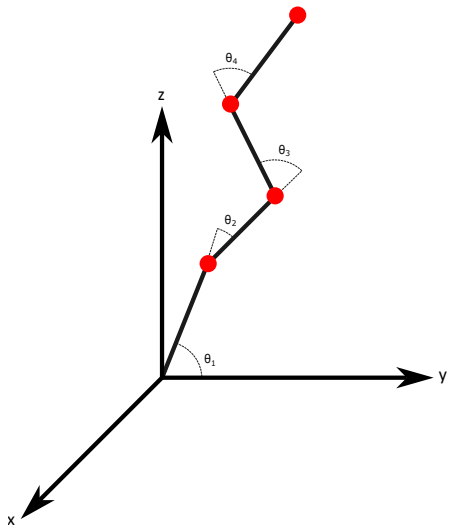

Figure 2.4: The Chain of Pendulums with angles between the pendulums as θ.

To model a beam, the concept of a spherical pendulum is extended to a chain of pendulums. Figure 2.4 illustrates this chain. Let $q = (q_1, \ldots, q_n) \in (S^2)^n$ be the attitude vector of the pendulums, where $q_i \in S^2$ represents the attitude vector of pendulum i. The masses are denoted $m_1, \ldots, m_n$, and the lengths $l_1, \ldots, l_n$. The coordinates of the mass of pendulum i is then described as the sum of the lengths of all preceding pendulums multiplied by their respective attitude vectors

$$r_i = \sum_{j=1}^{i} l_j q_j \quad \text{for } i = 1, \ldots, n.$$

This is used to derive the kinetic energy of the system expressed by the attitude vectors

$$K(\dot{q}) = \frac{1}{2} \dot{q}^T M \dot{q},$$

where the constant mass matrix M is [8]

$$M = \begin{bmatrix} M_{11}l_1^2 I_{3\times3} & M_{12}l_1l_2 I_{3\times3} & \dots & M_{1n}l_1l_n I_{3\times3} \\ M_{21}l_2l_1 I_{3\times3} & M_{22}l_2^2 I_{3\times3} & & \vdots \\ \vdots & & \ddots & \\ M_{n1}l_nl_1 I_{3\times3} & \dots & & M_{nn}l_n^2 I_{3\times3} \end{bmatrix},$$

with

$$M_{ij} = \sum_{k=\max\{i,j\}}^{n} m_k, \quad i,j = 1,\dots,n.$$

The mass matrix accounts for the distribution of mass and the lengths of the pendulums. Further, the gravitational energy of pendulum i is expressed as

$$E_i^G = m_i g \left(e_3^T r_i + \sum_{j=1}^{i} l_j \right) = \sum_{j=1}^{i} m_i g l_j (e_3^T q_j + 1).$$

The elastic energies of the springs follow the same form as in the single pendulum case. This results in the Lagrangian

$$L(q,\dot{q}) = \frac{1}{2}\dot{q}^T M \dot{q} - \sum_{i=1}^{n}\sum_{j=1}^{i} m_i g l_j (e_3^T q_j + 1) - \frac{1}{2}\sum_{i=1}^{n} k_i \arccos^2(q_{i-1}^T q_i),$$

where q_0 is the constant initial vector the first spring is attached to. To convert to the Hamiltonian, we require the conjugate moment. This is expressed by

$$p = \frac{\partial L}{\partial \dot{q}} = M\dot{q} \iff \dot{q} = M^{-1}p.$$

The Hamiltonian of the chain of pendulums restrained by springs in a gravitational field is then defined by

$$H(q,p) = \frac{1}{2}p^T M^{-1} p + \sum_{i=1}^{n}\sum_{j=1}^{i} m_i g l_j (e_3^T q_j + 1) + \frac{1}{2}\sum_{i=1}^{n} k_i \arccos^2(q_{i-1}^T q_i).$$

To apply the RATTLE method (1.6.1) to this system, we need the partial derivatives of the Hamiltonian, along with the constraints and the respective Jacobians. For ease of notation, we express the terms in the partial derivative of the elastic energy as

$$\frac{d}{dq_i}\left(\frac{1}{2}k_i \arccos^2\left(q_{i-1}^T q_i\right)\right) = -k_i \frac{\arccos\left(q_{i-1}^T q_i\right)}{\sqrt{1-\left(q_{i-1}^T q_i\right)^2}} q_{i-1} = -k_i s\left(q_{i-1}, q_i\right) q_{i-1},$$

where

$$s\left(q_{i-1}, q_i\right) = \frac{\arccos\left(q_{i-1}^T q_i\right)}{\sqrt{1-\left(q_{i-1}^T q_i\right)^2}}.$$

Note that when the pendulums are parallel, i.e. $q_{i-1}^T q_i = 1$, $s\left(q_{i-1}, q_i\right)$ is a zero over zero expression. However, through L'Hopital's rule we find the limit

$$\lim_{x\to1}\left(\frac{(\arccos(x))'}{(\sqrt{1-x^2})'}\right) = \lim_{x\to1}\left(\frac{-\frac{1}{\sqrt{1-x^2}}}{-\frac{x}{\sqrt{1-x^2}}}\right) = \lim_{x\to1}\left(\frac{1}{x}\right) = 1. \tag{2.2.1}$$

In the case of antiparallel pendulums, i.e. $q_{i-1}^T q_i = -1$, the corresponding term becomes $\frac{\pi}{0}$. However, this is an infeasible configuration of the system since it implies the beam has folded in over itself. Additionally, as the angles increase from zero to π, the forces penalizing them increases to infinity. Therefore, with suitably small step sizes, these configurations are not reached.

The partial derivatives of the Hamiltonian for the chain of pendulums restrained by springs in a gravitational field are then expressed as

$$\frac{\partial H}{\partial p} = M^{-1}p$$
$$\frac{\partial H}{\partial q} = \begin{bmatrix} \sum_{i=1}^{n} m_i g l_1 e_3 \\ \sum_{i=2}^{n} m_i g l_2 e_3 \\ \vdots \\ m_n g l_n e_3 \end{bmatrix} - \begin{bmatrix} k_1 s(q_0, q_1) q_0 + k_2 s(q_1, q_2) q_2 \\ k_2 s(q_1, q_2) q_1 + k_3 s(q_2, q_3) q_3 \\ \vdots \\ k_n s(q_{n-1}, q_n) q_{n-1} \end{bmatrix}.$$

Additionally, the length constraints of the n pendulums lead to the n constraint equations

$$g(q) = \begin{bmatrix} \frac{1}{2}(\|q_1\|^2 - 1) \\ \frac{1}{2}(\|q_2\|^2 - 1) \\ \vdots \\ \frac{1}{2}(\|q_n\|^2 - 1) \end{bmatrix},$$

and the corresponding Jacobian is the $n \times 3n$-matrix

$$G(q) = \begin{bmatrix} q_1^T & & & \\ & q_2^T & & \\ & & \ddots & \\ & & & q_n^T \end{bmatrix},$$

with zeros in all other positions.

2.2.3 Generalized Force

As observed in the derivation of the Euler-Bernoulli beam, Section 2.1.1, gravity is not the only force considered in beam theory. To account for other external forces, we generalize by again considering work. Work is defined as the product of force and displacement, and in the context of beams, it corresponds to the force multiplied by the displacement from the neutral axis. The beam configuration we focus on is the horizontal beam in the yz-plane, attached at the origin, affected by transverse forces in the same plane. The displacement is thus isolated to this plane and is the distance from the neutral axis $x = z = 0$. This configuration is the one considered throughout the thesis.

In terms of the chain of pendulums, the work done by a transverse force F_k in the yz-plane at pendulum k can be expressed as a potential energy term

$$W_k = F_k z_k = F_k \sum_{i=1}^{k} l_i e_3^T q_i.$$

As the respective energy term of the force can be expressed as a potential energy, the force is conservative and the Hamiltonian retains its preservation of energy. The total work done by external forces $F_1, \ldots, F_n$ on the entire chain is then expressed as

$$W = \sum_{k=1}^{n} F_k \sum_{i=1}^{k} l_i e_3^T q_i.$$

Considering the effect of external forces F_k at node k, the Hamiltonian of the chain of pendulums restrained by springs can be modified as follows

$$H(q,p) = \frac{1}{2} p^T M^{-1} p + \sum_{k=1}^{n} F_k \sum_{i=1}^{k} l_i e_3^T q_i + \frac{1}{2} \sum_{i=1}^{n} k_i \arccos^2(q_{i-1}^T q_i). \tag{2.2.2}$$

This leads to the generalized Hamiltonian equations for a chain of pendulums restrained by springs

$$\begin{aligned}\frac{\partial H}{\partial p} &= M^{-1}p \\ \frac{\partial H}{\partial q} &= \begin{bmatrix} \sum_{k=1}^{n} F_k l_1 e_3 \\ \sum_{k=2}^{n} F_k l_2 e_3 \\ \vdots \\ F_n l_n e_3 \end{bmatrix} - \begin{bmatrix} k_1 s(q_0, q_1) q_0 + k_2 s(q_1, q_2) q_2 \\ k_2 s(q_1, q_2) q_1 + k_3 s(q_2, q_3) q_3 \\ \vdots \\ k_n s(q_{n-1}, q_n) q_{n-1} \end{bmatrix},\end{aligned} \tag{2.2.3}$$

with the same constraints $g(q)$ as in the previous section. This is henceforth referred to as the Chain of Pendulums model. As the current configuration of the model is fixed in the origin, and the other end is freely hanging, it is a so called Cantilever beam. The same approach can be applied to account for transverse forces in the xy- and xz-plane to generalize the system further. This is left for future work.

2.2.4 Numerical Experiments

We now explore some numerical experiments. The general model we consider consists of $n = 10$ pendulums, each with a length $l = 1$ m and a spring constant $k = 10^3$ Nm/rad. An external force $F = 2$ N is applied to the tenth and final node.

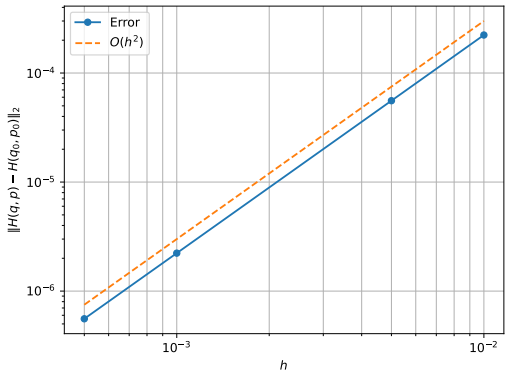

Figure 2.5: Norm of energy error of the Cantilever beam for different step sizes.

To begin with, we investigate the implementation of the RATTLE method (1.6.1) by examining the energy error relative to the step size. As the RATTLE method is of order $O(h^2)$, we expect a convergence plot to follow the same order. Figure 2.5 shows the norm of the energy error for different step sizes, exhibiting an order of $O(h^2)$ as expected, confirming the correctness of the implementation.

The evolution of the system is shown in Figure 2.6. Animation of this system can also be found here. The system evolves as expected of a Cantilever beam affected by a force in the final node, where the final node achieves the highest deflection, followed by the preceding nodes, before returning to the initial configuration.

As the system is Hamiltonian with conservative forces and holonomic constraints, we expect from Section 1.5 that the energy is conserved. This can be seen in Figure 2.7, confirming the conservation of energy by the Chain of Pendulums model (2.2.3).

Figure 2.8(left) presents an alternative representation of the trajectory. It illustrates the trajectories of each individual node, showing that the position of node i is the sum of the preceding nodes and the pendulum i itself. However, Figure 2.8(right) is the most notable, as it compares the trajectories of the final node of six different systems with a varying number of pendulums n. Despite the total length of the beam being constant at 10 m, the trajectories suggest a decrease in stiffness as the number of nodes increases. This observation indicates that the spring constant k does not always directly translate to the flexural rigidity EI of beams.

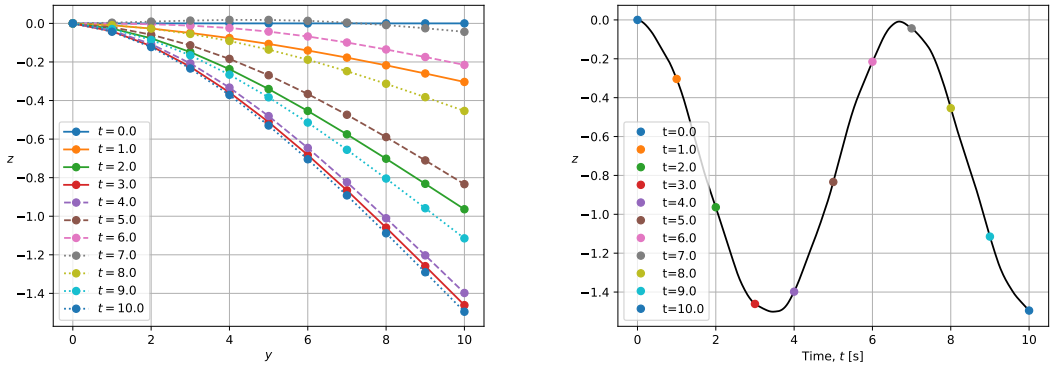

Figure 2.6: Trajectory of the Cantilever beam modeled by the Chain of Pendulums model (2.2.3) affected by a point load in the final node. Left: Configurations of the beam at different times. Solid lines represent the initial translation down, dashed lines on the way up, and dotted lines on the second translation down. Right: Trajectory of the final node, with intermediate times corresponding to the left plot.

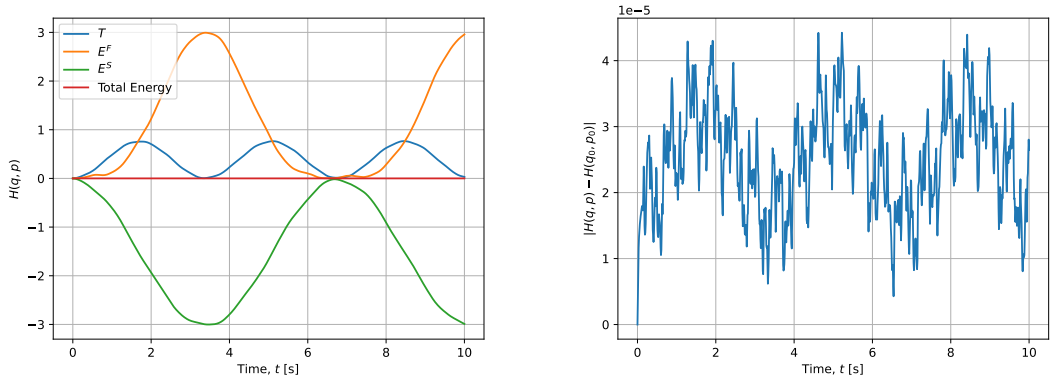

Figure 2.7: Energy of the Cantilever beam modeled by the Chain of Pendulums model (2.2.3) affected by a point load in the final node. Left: Total energy of the system, including the kinetic energy T, spring energy E^S, and energy from the force applied to the final node E^F. Right: Error in energy.

2.3 Comparison of the Models

Having established our Chain of Pendulums beam model (2.2.3), it would be insightful to compare it to the commonly used Euler-Bernoulli beam model (2.1.5) to investigate similarities and differences. One of the main differences of the models is that while the Euler-Bernoulli beam is continuous, the Chain of Pendulums model is discrete. Thus, to compare we discretize the Euler-Bernoulli beam.

Consider the space discretization of the Euler-Bernoulli equation (2.1.5) with finite differences,

$$\mu \begin{bmatrix} \vdots \\ \ddot{z}_{i-2} \\ \ddot{z}_{i-1} \\ \ddot{z}_i \\ \ddot{z}_{i+1} \\ \ddot{z}_{i+2} \\ \vdots \end{bmatrix} = -\frac{EI}{d^4} \begin{bmatrix} \ddots & \vdots & \vdots & \vdots & \vdots & \vdots & \vdots & \vdots & \vdots & \vdots & \\ \dots & 1 & -4 & 6 & -4 & 1 & 0 & 0 & 0 & 0 & \dots \\ \dots & 0 & 1 & -4 & 6 & -4 & 1 & 0 & 0 & 0 & \dots \\ \dots & 0 & 0 & 1 & -4 & 6 & -4 & 1 & 0 & 0 & \dots \\ \dots & 0 & 0 & 0 & 1 & -4 & 6 & -4 & 1 & 0 & \dots \\ \dots & 0 & 0 & 0 & 0 & 1 & -4 & 6 & -4 & 1 & \dots \\ & \vdots & \vdots & \vdots & \vdots & \vdots & \vdots & \vdots & \vdots & \vdots & \ddots \end{bmatrix} \begin{bmatrix} \vdots \\ z_{i-2} \\ z_{i-1} \\ z_i \\ z_{i+1} \\ z_{i+2} \\ \vdots \end{bmatrix} + \begin{bmatrix} \vdots \\ w_{i-2} \\ w_{i-1} \\ w_i \\ w_{i+1} \\ w_{i+2} \\ \vdots \end{bmatrix}, \tag{2.3.1}$$

where the first three and final three nodes are dealt with by considering boundary conditions as

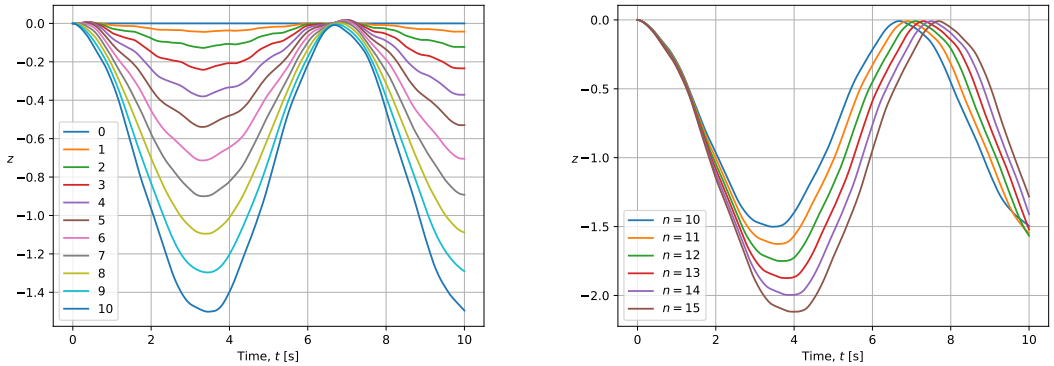

Figure 2.8: Trajectories of the Cantilever beam modeled by the Chain of Pendulums model (2.2.3) affected by a point load in the final node. Left: Trajectories of each individual node, with $n = 10$ pendulums. Right: Trajectories of the final node of six different systems with consistent total length $L = 10$ m, but with increasing amount of nodes.

in [18]. The equations of motion for the Chain of Pendulums model (2.2.3) given in terms of the conjugate moment p is

$$\dot{p} = M\ddot{q} = \begin{bmatrix} k_1 s(q_0, q_1) q_0 + k_2 s(q_1, q_2) q_2 \\ k_2 s(q_1, q_2) q_1 + k_3 s(q_2, q_3) q_3 \\ \vdots \\ k_n s(q_{n-1}, q_n) q_{n-1} \end{bmatrix} - \begin{bmatrix} \sum_{k=1}^{n} F_k l_1 e_3 \\ \sum_{k=2}^{n} F_k l_2 e_3 \\ \vdots \\ F_n l_n e_3 \end{bmatrix} - \begin{bmatrix} \lambda_1 q_1 \\ \lambda_2 q_2 \\ \vdots \\ \lambda_n q_n \end{bmatrix}. \tag{2.3.2}$$

Note that this is a model consisting of all three components, x, y, and z. The consideration of three components versus one is a definition difference. As we have seen, the Euler-Bernoulli beam is capable of accomodating transverse loads in an additional direction, as well as axial loads. Conversely, the Chain of Pendulums system (2.3.2) is formulated for only transverse loads in the vertical component, hence the e_3 in the force term to account for the transverse force as it is applied in the z-axis. Thus, it is an amicable comparison of the two models, as they are both affected by transverse forces acting in a single plane.

Now, considering that $\ddot{z}_i$ is the acceleration of the nodes in the Euler-Bernoulli system (2.3.1), we reformulate the Chain of Pendulums system (2.3.2) in order to derive the expressions for the acceleration of the nodes, $\ddot{r}$. This is done by expanding $M\ddot{q}$,

$$\begin{aligned} \dot{p} = M\ddot{q} &= \begin{bmatrix} \sum_{i=1}^{n} m_i l_1^2 \ddot{q}_1 + \sum_{i=2}^{n} m_i l_1 l_2 \ddot{q}_2 + \cdots + m_n l_1 l_n \ddot{q}_3 \\ \sum_{i=2}^{n} m_i l_2 l_1 \ddot{q}_1 + \sum_{i=2}^{n} m_i l_2^2 \ddot{q}_2 + \sum_{i=3}^{n} m_i l_2 l_3 \ddot{q}_3 + \cdots + m_n l_2 l_n \ddot{q}_n \\ \vdots \\ m_n l_n l_1 \ddot{q}_1 + m_n l_n l_2 \ddot{q}_2 + \cdots + m_n l_n^2 \ddot{q}_n \end{bmatrix} \\ &= \begin{bmatrix} l_1 \left(m_1 l_1 \ddot{q}_1 + m_2 (l_1 \ddot{q}_1 + l_2 \ddot{q}_2) + \cdots + m_n (l_1 \ddot{q}_1 + \cdots + l_n \ddot{q}_n) \right) \\ l_2 (m_2 (l_1 \ddot{q}_1 + l_2 \ddot{q}_2) + \cdots + m_n (l_1 \ddot{q}_1 + \cdots + l_n \ddot{q}_n) \\ \vdots \\ l_n (m_n (l_1 \ddot{q}_1 + \cdots + l_n \ddot{q}_n)) \end{bmatrix} \\ &= \begin{bmatrix} l_1 (m_1 \ddot{r}_1 + m_2 \ddot{r}_2 + \cdots + m_n \ddot{r}_n) \\ l_2 (m_2 \ddot{r}_2 + \cdots + m_n \ddot{r}_n) \\ \vdots \\ l_n (m_n \ddot{r}_n) \end{bmatrix}. \end{aligned}$$

Now working from p_n to p_1 we get a nice expression

$$\begin{aligned}
\dot{p}_n &= l_n m_n \ddot{r}_n && \implies m_n \ddot{r}_n = \frac{\dot{p}_n}{l_n} \\
\dot{p}_{n-1} &= l_{n-1}(m_{n-1}\ddot{r}_{n-1} + m_n \ddot{r}_n) && \implies m_{n-1}\ddot{r}_{n-1} = \frac{\dot{p}_{n-1}}{l_{n-1}} - \frac{\dot{p}_n}{l_n} \\
\dot{p}_{n-2} &= l_{n-2}(m_{n-2}\ddot{r}_{n-2} + m_{n-1}\ddot{r}_{n-1} + m_n \ddot{r}_n) && \implies m_{n-2}\ddot{r}_{n-2} = \frac{\dot{p}_{n-2}}{l_{n-2}} - \frac{\dot{p}_{n-1}}{l_{n-1}} + \frac{\dot{p}_n}{l_n} - \frac{\dot{p}_n}{l_n} \\
& && = \frac{\dot{p}_{n-2}}{l_{n-2}} - \frac{\dot{p}_{n-1}}{l_{n-1}} \\
& && \vdots \\
\dot{p}_2 &= l_2(m_2\ddot{r}_2 + \cdots + m_n \ddot{r}_n) && \implies m_2 \ddot{r}_2 = \frac{\dot{p}_2}{l_2} - \frac{\dot{p}_3}{l_3} \\
\dot{p}_1 &= l_1(m_1\ddot{r}_1 + \cdots + m_n \ddot{r}_n) && \implies m_1 \ddot{r}_1 = \frac{\dot{p}_1}{l_1} - \frac{\dot{p}_2}{l_2}
\end{aligned}$$

By substituting these relations into the equations of motion for the Chain of Pendulums system (2.3.2), we find that the equations of motion for the nodes in the Chain of Pendulums model (2.2.3) are

$$\begin{aligned}
m\ddot{r} = &\begin{bmatrix} \frac{1}{l_1}\left(k_1 s(q_0,q_1)q_0 + k_2 s(q_1,q_2)q_2\right) - \frac{1}{l_2}\left(k_2 s(q_1,q_2)q_1 + k_3 s(q_2,q_3)q_3\right)) \\ \frac{1}{l_2}\left(k_2 s(q_1,q_2)q_1 + k_3 s(q_2,q_3)q_3\right) - \frac{1}{l_3}\left(k_3 s(q_2,q_3)q_2 + k_4 s(q_3,q_4)q_4\right)) \\ \vdots \\ \frac{1}{l_n} k_n s(q_{n-1},q_n) q_{n-1} \end{bmatrix} \\
&- \begin{bmatrix} F_1 e_3 \\ F_2 e_3 \\ \vdots \\ F_n e_3 \end{bmatrix} - \begin{bmatrix} \frac{\lambda_1}{l_1}q_1 - \frac{\lambda_2}{l_2}q_2 \\ \frac{\lambda_2}{l_2}q_2 - \frac{\lambda_3}{l_3}q_3 \\ \vdots \\ \frac{\lambda_n}{l_n}q_n \end{bmatrix},
\end{aligned} \tag{2.3.3}$$

where m is the diagonal mass matrix.

We investigate the systems term by term and compare them. If we let the mass of each pendulum be equal, m is simply the mass per pendulum length, equal to μ in the Euler-Bernoulli system (2.3.1). On the left-hand side of the Chain of Pendulums system (2.3.3) we thus have the product of the mass and acceleration of the nodes, which is equal to the left-hand side of the Euler-Bernoulli system.

Furthermore, if we let the spring constants k_i be equal one another, and the pendulum lengths l_i as well, we can extract them from the vector. In the Euler-Bernoulli system (2.3.1), the equivalent is EI/d^4. Thus, in both systems we have a constant that incorporates the rigidity and discretization of the systems. This constant is multiplied by a vector of functions of positions, and as we have seen, in both of the equations, these functions of positions can be related back to the same angles. As the Euler-Bernoulli beam (2.1.5) is linear, these consist of linear terms, while the Chain of Pendulums system (2.3.3) terms are nonlinear in the positions.

The force term in the Chain of Pendulums system (2.3.3) consists purely of the point-forces affecting each node, equivalent to the force term in the Euler-Bernoulli system (2.3.1). Thus, the difference between the models in this discretization is the non-linearity in the elasticity terms, as well as the reaction forces serving to constrain the pendulum lengths. If we expand Euler-Bernoulli back into considering transverse forces in two planes, as well as applying forces in two planes for the Chain of Pendulums, the similarities are expected to still hold. However, when axial loads are introduced, the constraints in the Chain of Pendulums prevents it from expanding, something Euler-Bernoulli is able to account for. However, as discussed before, in rigid rods and long, thin beams affected by transverse loads, we are often only concerned by the response in the transverse direction. To account for axial loads in the Chain of Pendulums, one potential approach could be to replace the rigid pendulums by springs. This is not considered in this thesis.

As mentioned, it is important to note that the Euler-Bernoulli beam (2.1.5) is a continuous model. However, even then, the comparisons hold as both the Chain of Pendulums system (2.3.3) and Euler-Bernoulli beam is of the form mass times acceleration equal to a term concerning elasticity and a term concerning force, where there is an additional term in the Chain of Pendulums

system concerning the length constraints.

2.3.1 Numerical Comparison

To compare the two models numerically, we consider the same Cantilever beam as previously discussed. In both the Chain of Pendulums model (2.2.3) and the Euler-Bernoulli beam (2.1.5), we use equivalent parameters. Specifically, the point masses and length of discretization are set equal, while the spring constants are considered equal to the flexural rigidity, $k = 10^3$ Nm/rad, $EI = 10^3$ Nm^2. The force $F = 2$ N is applied to the final node. Note that with $n = 10$ pendulums, the system consists of 11 nodes counting the origin. This is considered the zeroth node.

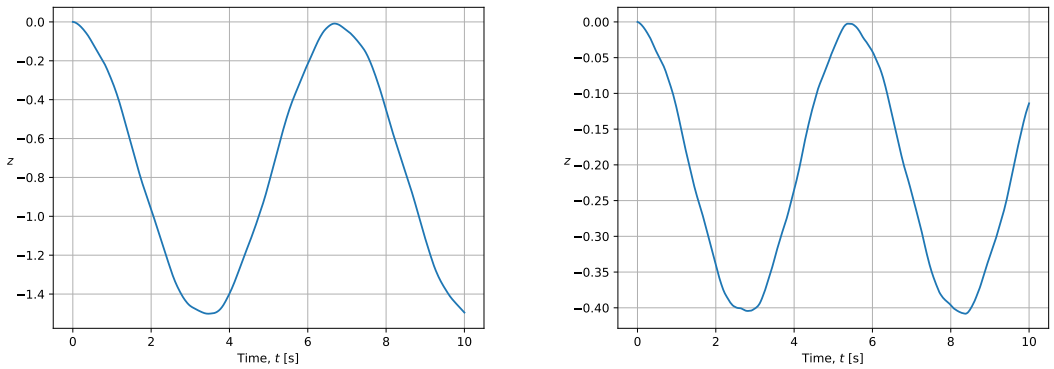

Figure 2.9: Trajectories of the final node of the Cantilever beam modeled by the Chain of Pendulums model (2.2.3) and the Euler-Bernoulli beam (2.1.5) affected by a point load in the final node. Left: Chain of Pendulums. Right: Trajectory of the Euler-Bernoulli.

We compare the trajectory of the final node. This is shown in Figure 2.9 and animations of the systems can be found here. There are obvious differences. The rigidity of the Euler-Bernoulli beam (2.1.5) appears higher as the resulting magnitude of the deflection is lower. This is not too unexpected, as it was illustrated in Figure 2.8 that the spring constant in the Chain of Pendulums model (2.2.3) does not directly translate to the rigidity of a beam. Additionally, the period of oscillation of the Chain of Pendulums model is longer, which through experimentation has been determined to be influenced by both mass and the spring constant. This difference will later be shown to be an error attributed to the implementation of the freely hanging end of the Euler-Bernoulli beam. However, the general qualitative trajectory is similar, and by adjusting the parameters of the Chain of Pendulums model it is possible to achieve a closer approximation to this implementation of the Euler-Bernoulli model.

By setting the spring constant to $k = 1.16 \times 10^3$ Nm/rad and the mass of each pendulum to be $m = 2.4$ kg in the Chain of Pendulums model (2.2.3), we obtain the trajectories as depicted in Figure 2.10. These parameter values are chosen as they give the best correlation in the node with the highest displacement. Note that these parameters are determined through trial and error, and other configurations might lead to even better overall results. The trajectories of the nodes closer to the fixed point in the Euler-Bernoulli model (2.1.5) appear to still be more rigid than the nodes of the Chain of Pendulums model. However, the trajectories follow the same qualitative behavior, and the final nodes seem to mimic each other well. Thus, the Chain of Pendulums model seems feasible to model the Cantilever beam by carefully choosing the parameters.

2.4 Extending Properties

The current configuration of the Chain of Pendulums model (2.2.3) represents the properties of a Cantilever beam in vacuum. However, there exists beam configurations beyond the fixed-free Cantilever setup. Additionally, real-life beam applications can involve non-conservative forces.

Given these considerations, we investigate if our model can be expanded to accommodate for beams with different properties. To achieve this, we extend the model to account for different beam supports by considering appropriate boundary conditions at the zeroth and final nodes.

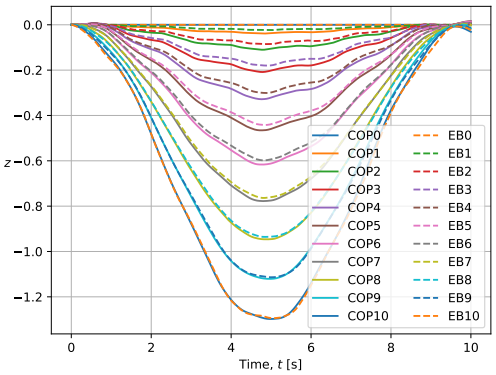

Figure 2.10: Trajectory of the nodes of the Cantilever beam modeled by the Chain of Pendulums model (2.2.3) and the Euler-Bernoulli model (2.1.5) affected by a point load in the final node. The mass and spring constant used in the Chain of Pendulums model are respectively $m = 2.4$ kg and $k = 1.16 \times 10^3$ Nm/rad, per pendulum. The mass used in the Euler-Bernoulli model is $m = 1$ kg per node, and the flexural rigidity is $EI = 3.125 \times 10^2$ Nm^2.

Additionally, in order to demonstrate the capability of the model to include non-conservative forces, despite being built upon Hamiltonian principles, we introduce drag by including it in the equations of motion.

2.4.1 Boundary Constraints

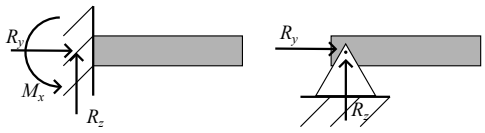

Figure 2.11: Beam supports and the reaction forces and moment that can represent them. Left: Fixed. Right: Pinned.

To demonstrate that it is possible to further develop the Chain of Pendulums model (2.2.3) to account for different types of beams, we consider boundary constraints. Various types of boundary conditions, or supports, exist for beams [19]. We focus on three types, *fixed*, *pinned*, and *free*. These supports can be modelled by forces and moment as illustrated in 2.11, where the free end is not affected by any.

1. Fixed support represents an anchored end that remains immobile and cannot rotate. This can be modeled as two forces and a moment acting on the endpoint.

2. Pinned support represents an end that is anchored, but free to rotate. This can be modeled as two forces acting on the end-point, preventing it from translating in the plane, but free to rotate.

3. Freely hanging means that there is no restriction on the movement or rotation of the end.

The beam considered so far is the Cantilever beam, which is fixed at one end, the origin, and free to move at the other. As we are interested in different configurations of beams, it is necessary to support the node at the freely hanging end. Both the fixed support and the pinned support requires the endpoint of the final pendulum to be not move. This can be achieved by introducing an additional constraint to ensure that the z-component of the final node remains zero,

$$l(q) = \sum_{i=1}^{n} l_i e_3^T q_i - r_n(t_0), \tag{2.4.1}$$

where $r_n(t_0)$ denotes the initial z-coordinate of the final node. Adding this to the length constraints yields $\hat{g}(q) = \begin{bmatrix} g(q)^T & l(q) \end{bmatrix}^T$. As the configuration considered is the horizontal beam, the initial configuration of the nodes lie on the y-axis, and such $r_n(t_0) = 0$. The Jacobian of the constraints thus gets another row,

$$\hat{G}(q) = \begin{bmatrix} G(q) \\ L(q) \end{bmatrix} = \begin{bmatrix} & & & & G(q) & & & & & \\ 0 & 0 & l_1 & 0 & 0 & l_2 & \dots & 0 & 0 & l_n \end{bmatrix}.$$

This constraint represents the reaction force acting in the z-direction. While it is also possible to impose restrictions in the x-direction, it is unnecessary for this application as we focus on transverse forces in the yz-plane. However, as mentioned in the description of the beam support and illustrated in Figure 2.11, the supports can be modeled by two forces. Thus, it is desirable to impose a restriction in the y-direction as well. However, if we restrict the y-coordinate of the final node and apply a force in the z-direction to any node, perpendicular to the y-direction, the pendulums have no feasible direction to move or configuration to obtain due to their constrained lengths and the locked y-coordinate of the final node.

However, as there is no applied force in the y-direction, the only movement in that direction arises from the pull of the pendulums in the transverse direction. This movement is relatively small compared to the movement in the z-direction, and it will be shown that the restriction in z-coordinate is sufficient for this application. Thus, with the reaction force in z-direction, the final component required to transform the Cantilever beam into a Fixed-Fixed beam is the addition of a term representing the reaction moment. This can be achieved by introducing a spring term between the final pendulum and a constant horizontal vector, as done in the origin. The equations of motion for a Fixed-Fixed beam are then

$$\begin{aligned} \dot{q} &= \frac{\partial H}{\partial p} = M^{-1}p \\ \dot{p} &= -\frac{\partial H}{\partial q} - \hat{G}(q)^T\hat{\lambda} \\ &= \begin{bmatrix} k_1 s(q_0,q_1)q_0 + k_2 s(q_1,q_2)q_2 \\ k_2 s(q_1,q_2)q_1 + k_3 s(q_2,q_3)q_3 \\ \vdots \\ k_n s(q_{n-1},q_n)q_{n-1} + k_{n+1} s(q_n,q_{n+1})q_{n+1} \end{bmatrix} - \begin{bmatrix} \sum_{k=1}^{n} F_k l_1 e_3 \\ \sum_{k=2}^{n} F_k l_2 e_3 \\ \vdots \\ F_n l_n e_3 \end{bmatrix} - \begin{bmatrix} \lambda_1 q_1 \\ \lambda_2 q_2 \\ \vdots \\ \lambda_n q_n \end{bmatrix} - \lambda_L \begin{bmatrix} l_1 e_3 \\ l_2 e_3 \\ \vdots \\ l_n e_3 \end{bmatrix}, \end{aligned} \tag{2.4.2}$$

where k_{n+1} represents the spring constant of the added spring, and q_{n+1} is the constant horizontal vector at the final node. The resulting Lagrangian multiplier associated with the boundary constraint of the z-coordinate is denoted λ_L.

The difference between a Fixed-Fixed beam and a Pinned-Pinned beam is the absence of a reaction moment in the latter. By removing the first and final spring terms, we obtain the equations of motion for the Pinned-Pinned beam

$$\begin{aligned} \dot{q} &= \frac{\partial H}{\partial p} = M^{-1}p \\ \dot{p} &= -\frac{\partial H}{\partial q} - \hat{G}(q)^T\hat{\lambda} \\ &= \begin{bmatrix} k_2 s(q_1,q_2)q_2 \\ k_2 s(q_1,q_2)q_1 + k_3 s(q_2,q_3)q_3 \\ \vdots \\ k_n s(q_{n-1},q_n)q_{n-1} \end{bmatrix} - \begin{bmatrix} \sum_{k=1}^{n} F_k l_1 e_3 \\ \sum_{k=2}^{n} F_k l_2 e_3 \\ \vdots \\ F_n l_n e_3 \end{bmatrix} - \begin{bmatrix} \lambda_1 q_1 \\ \lambda_2 q_2 \\ \vdots \\ \lambda_n q_n \end{bmatrix} - \lambda_L \begin{bmatrix} l_1 e_3 \\ l_2 e_3 \\ \vdots \\ l_n e_3 \end{bmatrix}. \end{aligned} \tag{2.4.3}$$

2.4.2 Numerical Experiments

We continue our comparison with the Euler-Bernoulli model by considering the Fixed-Fixed beam. As previously, the model consisting of $n = 10$ pendulums is used, and we apply the same parameters for both models, mass $m = 1$ kg and length $l = 1$ m per node. Note that the masses of the stationary nodes are not significant. The spring constant is set to be equal to the flexural rigidity, $k = 10^3$ Nm/rad, $EI = 10^3$ Nm^2, and a force $F = 2$ N is applied to the central node. The trajectories of the beams are shown in Figure 2.12, and animations of the systems can be found here.

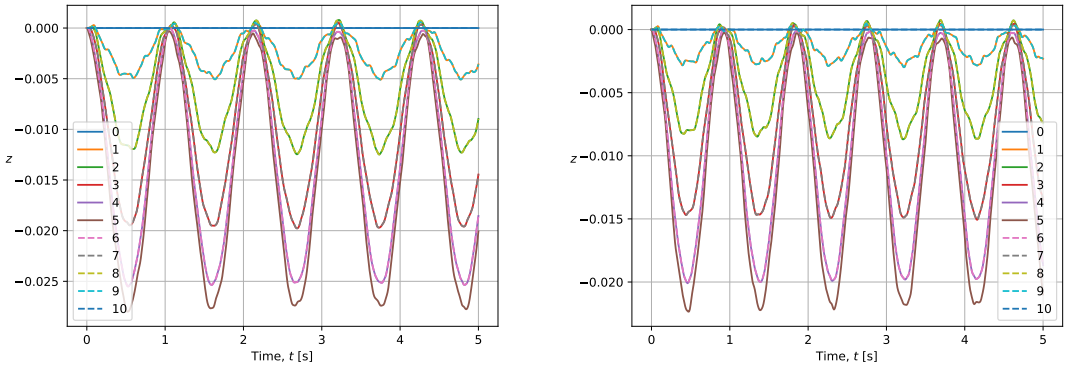

Figure 2.12: Trajectories of the nodes of the Fixed-Fixed beam modeled by the Chain of Pendulums model (2.4.2) and the Euler-Bernoulli beam model (2.1.5) affected by a point load in the central node. Solid lines represent the nodes left of, and including, the central node, dashed lines the ones to the right. Left: Chain of Pendulums model. Right: Euler-Bernoulli beam.

As with the Cantilever beam, the trajectories do not match exactly. The period of the oscillation is longer for the Chain of Pendulums model, and again the Euler-Bernoulli beam is more rigid. However, the evolution of the systems behave similarly, node by node. Notably, the trajectories of the nodes on each side of the central node are symmetric, as expected. To approximate the Euler-Bernoulli model better, we adjust the parameters of the Chain of Pendulums model.

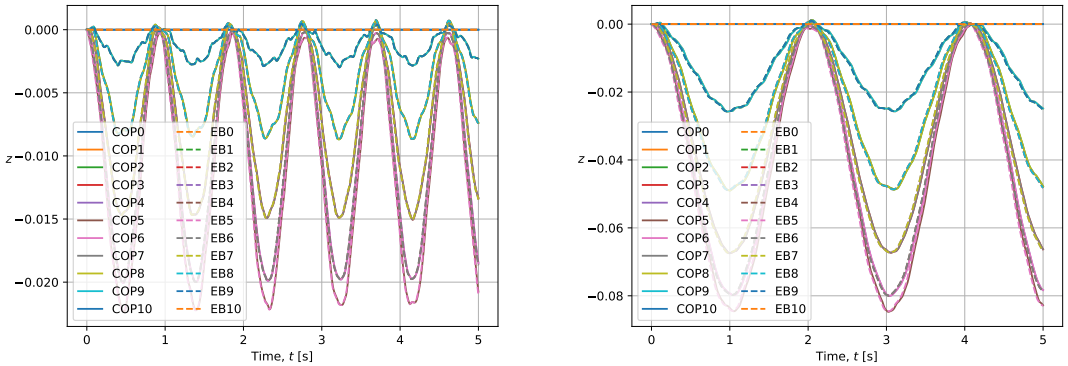

Figure 2.13: Trajectories of the nodes of the Fixed-Fixed and Pinned-Pinned beams modeled by the Chain of Pendulums model, (2.4.2) and (2.4.3) respectively, and the Euler-Bernoulli model (2.1.5) affected by a point load in the central node. The dashed lines describing the Euler-Bernoulli trajectories overlap with the Chain of Pendulums lines, showing equivalence. Left: Fixed-Fixed beam. Right: Pinned-Pinned beam.

Figure 2.13(left) displays the trajectories of the nodes using the adjusted parameters. By setting the spring constants in the zeroth and final nodes to $k_1 = k_{n+1} = 2 \times 10^3$ Nm/rad, the resulting trajectories of the Fixed-Fixed beam modeled by the Chain of Pendulums model is equivalent to the trajectories given by the Euler-Bernoulli beam.

When considering the Pinned-Pinned beam, the parameters are the same as used in the Fixed-Fixed beam, but the springs of the zeroth and final nodes are removed. The resulting trajectories of the models are shown in Figure 2.13(right). As observed, the models are equivalent, without changing any parameters.

Both the Fixed-Fixed and Pinned-Pinned beams, along with the Cantilever beam discussed in Section 2.3.1, demonstrate that the Chain of Pendulums model can simulate the behavior of the Euler-Bernoulli beam by appropriately selecting the parameters.

2.4.3 Dissipation

In mechanical systems, conservative forces are typically considered, neglecting the dissipation of energy that occurs in real systems.

The forces previously considered have been conservative. The total work done by a conservative force on a particle between two points is indepentent of the path taken. This allowed us to include those forces as potential terms in the Hamiltonian. On the other hand, for non-conservative forces, it is not possible to find a potential that results in the desired force term when differentiating it. However, forces like these can be incorporated by including them in the equations of motion of the system, similar to the constraints [20]

$$\begin{aligned}\dot{q} &= \frac{\partial H}{\partial p} \\ \dot{p} &= -\frac{\partial H}{\partial q} + f(q,p),\end{aligned}$$

where $f(q,p)$ is a non-conservative force.

To illustrate that our system can handle dissipative forces, we add a drag force,

$$F_D(v) = \frac{1}{2}\rho v^2 C_D A,$$

where ρ is the density of the fluid, v the velocity of the object relative to the fluid, C_D is a dimensionless drag coefficient, and A the cross sectional area of the object. We combine these constants into a single parameter, denoted D. As drag force acts in the opposite direction of the velocity of the object, we can rewrite the expression to account for the direction of the force as well [8]

$$F_D(v) = -Dv|v|.$$

By considering the conjugate momentum p, and letting D include all the constants, we obtain the equations of motion for the dissipative Chain of Pendulums model become

$$\begin{aligned}\dot{q} &= \frac{\partial H}{\partial p} = M^{-1}p \\ \dot{p} &= -\frac{\partial H}{\partial q} + F_D(p) - G(q)^T\lambda \\ &= \begin{bmatrix} k_1 s(q_0,q_1)q_0 + k_2 s(q_1,q_2)q_2 \\ k_2 s(q_1,q_2)q_1 + k_3 s(q_2,q_3)q_3 \\ \vdots \\ k_n s(q_{n-1},q_n)q_{n-1} + k_{n+1}s(q_n,q_{n+1})q_{n+1}\end{bmatrix} - \begin{bmatrix} \sum_{k=1}^{n} F_k l_1 e_3 \\ \sum_{k=2}^{n} F_k l_2 e_3 \\ \vdots \\ F_n l_n e_3 \end{bmatrix} \\ &\quad - D\begin{bmatrix} p_1 \odot |p_1| \\ p_2 \odot |p_2| \\ \vdots \\ p_n \odot |p_n| \end{bmatrix} - \begin{bmatrix} \lambda_1 q_1 \\ \lambda_2 q_2 \\ \vdots \\ \lambda_n q_n \end{bmatrix},\end{aligned} \tag{2.4.4}$$

where $|\cdot|$ is elementwise absolute value, and $\odot$ is elementwise multiplication. Note that by replacing the constraint $g(q)$ and its Jacobian $G(q)$ by the extended constraint $\hat{g}(q)$ and its Jacobian $\hat{G}(q)$, and considering the spring constants of the zeroth and the final node k_0 and k_{n+1}, we can obtain the dissipative models for the different configurations.

2.4.4 Numerical Experiments

To investigate if the system containing dissipation terms is reasonable, we explore it numerically. As energy dissipates from the system, the nodes eventually reach a static configuration, which can be compared to the static solution of a beam under load. The expressions describing the deflection of beams with different supports affected by a point load are as follows [21]

Static Cantilever:

$$z = -F\frac{y^2}{6EI}(3L - y) \tag{2.4.5}$$

Static Fixed-Fixed:

$$\begin{aligned} z &= -F\frac{y^2}{48EI}\left(3L-4y\right) && \text{for } y \leq L \\ z &= -F\frac{(L-y)^2}{48EI}\left(3L-4(L-y)\right) && \text{for } y > L \end{aligned} \tag{2.4.6}$$

Static Pinned-Pinned:

$$\begin{aligned} z &= F\frac{y}{48EI}\left(3L^2-4y^2\right) && \text{for } y \leq L \\ z &= F\frac{(L-y)}{48EI}\left(3L^2-4(L-y)^2\right) && \text{for } y > L \end{aligned} \tag{2.4.7}$$

The Cantilever is affected by a point load in the final node, while the Fixed-Fixed and Pinned-Pinned beams are affected by a point load in the central node.

Figure 2.14 shows the trajectories of the nodes of the different beams modeled by the dissipative Chain of Pendulums model (2.4.4). Animations of the systems can be found here. The beams are implemented with the same parameters as before, where a fixed support constitutes $k_0 = k_{n+1} = 2 \times 10^3$ Nm/rad and a pinned support $k_0 = k_{n+1} = 0$. Two different dissipation constants are applied, $D = 10$ kg/m in the left column and $D = 100$ kg/m in the right column. A higher constant results in faster and more significant dissipation. The nodes follow the static solutions given by equations (2.4.5), (2.4.6), and (2.4.7), although settling overall lower.

Figure 2.15 illustrates the similarities between the dissipative Chain of Pendulums model (2.4.4) and the static solutions. The resulting beam configurations of the dissipative Chain of Pendulums model seem to resemble their respective static solutions, (2.4.5), (2.4.6), and (2.4.7), well, with the Fixed-Fixed beam being less stiff than expected.

As observed in Section 2.3.1, while they shared the same qualitative behavior, there was a significant difference between the Cantilever beam given by the Chain of Pendulums model (2.2.3) and the Euler-Bernoulli beam (2.1.5). However, the implementation of the dissipative Cantilever beam here follows its static solution to a degree that indicates an error in the implementation of the Euler-Bernoulli model in Section 2.3.1. In fact, when comparing the solution of the Cantilever beam given by the implementation of the static Euler-Bernoulli equation (2.1.4) to the static Cantilever equation (2.4.5), there is also a discrepancy. This is shown in Figure 2.16. On the other hand, the results of the Fixed-Fixed and Pinned-Pinned beams in Section 2.4.2 correlated well with the Euler-Bernoulli model. Furthermore, the dissipative Chain of Pendulums beams correlate well with their static solutions here. The Cantilever beam is the only one consisting of a freely hanging end, and as that is the only configuration where the Euler-Bernoulli beam exhibits different results than our model and the static equations, this suggests that the error in Section 2.3.1 is due to the implementation of the freely hanging end of the Euler-Bernoulli beam. Thus, the Chain of Pendulums again seems feasible to model beams, including dissipative terms.

An aspect that is not explored here, but could be an interesting idea for future development of this work, is the convergence of the models as the discretization n tends to infinity. It would be valuable to explore whether the considered discretization with finite differences of the Euler-Bernoulli beam (2.3.1), and similarly the Chain of Pendulums model (2.4.4), converge each to its own continuous model, or if they become unstable. While we do not expect that they converge to the same model, each of these discrete models should converge to a continuous model. This is particularly interesting for the Chain of Pendulums, which is conceived as a discrete model.

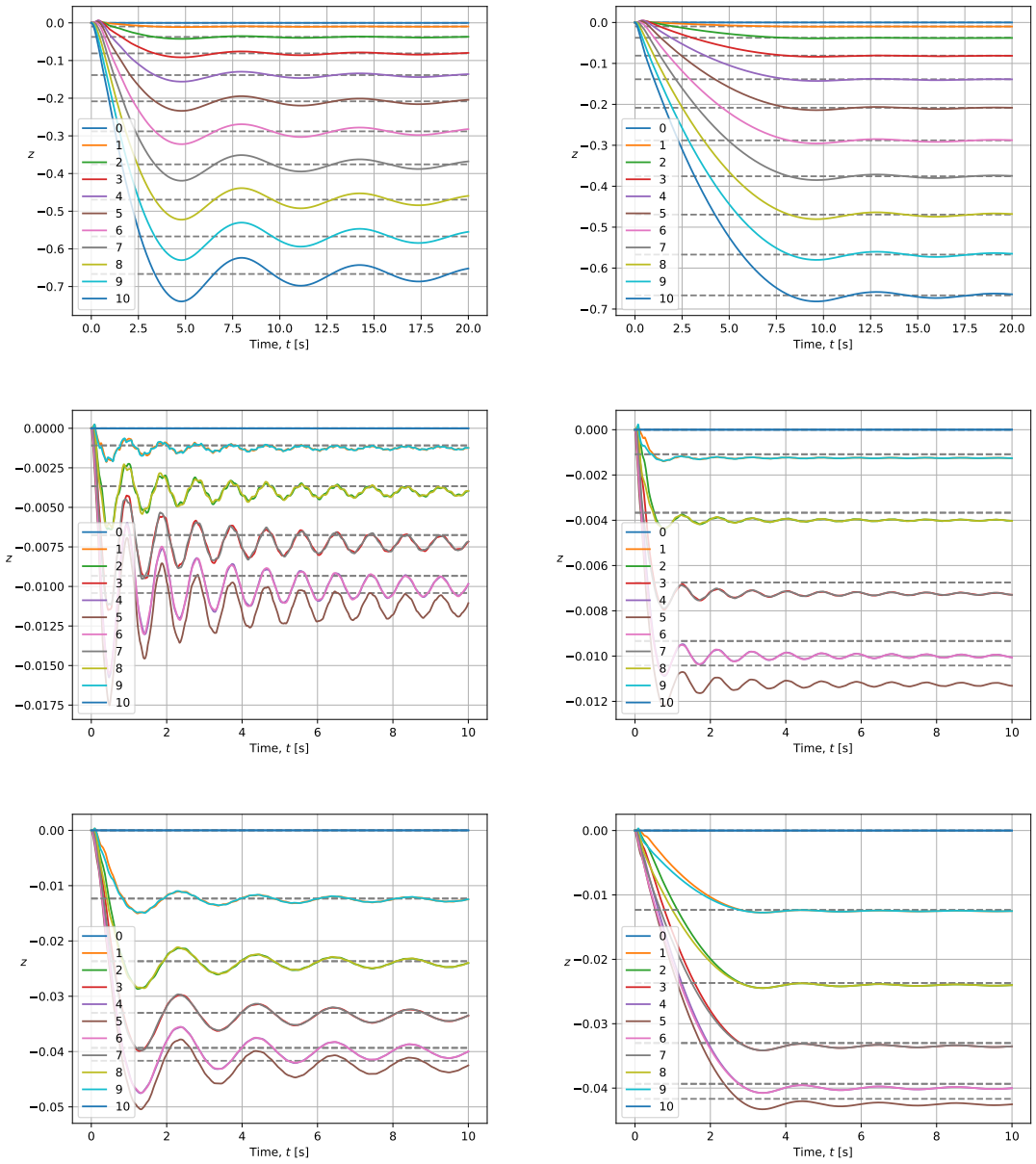

Figure 2.14: Trajectories of the nodes of the beams modeled by the dissipative Chain of Pendulums model (2.4.4). The model is implemented with two different dissipation constants $D = 10$ kg/m, left column, and $D = 100$ kg/m, right column. The first row contains the trajectory of the nodes of the Cantilever beam, the second row the Fixed-Fixed beam, and the final row the Pinned-Pinned beam. The dashed grey lines are the static solutions given by equations (2.4.5), (2.4.6), and (2.4.7).

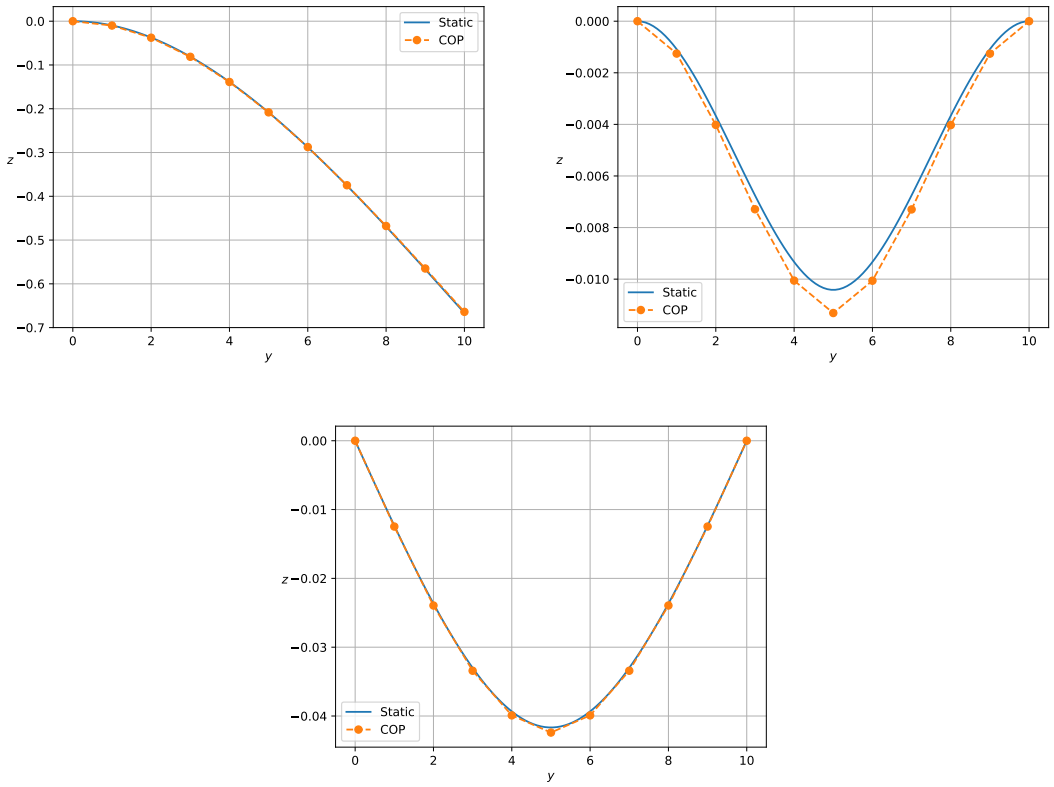

Figure 2.15: Static configuration of the beams modeled by the dissipative Chain of Pendulums model (2.4.4). The top left figure shows the Cantilever beam, the top right the Fixed-Fixed beam, and the bottom the Pinned-Pinned beam. The solution configurations given by equations (2.4.5), (2.4.6), and (2.4.7) are shown in blue.

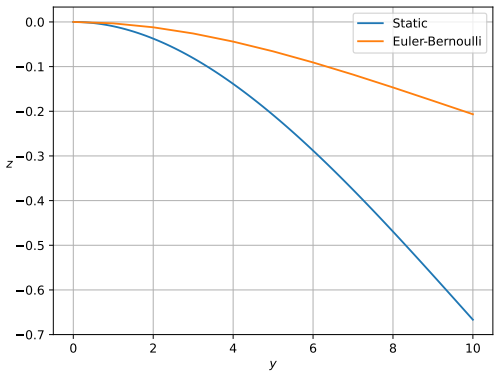

Figure 2.16: Static Cantilever beam (2.4.5) and solution of the static Euler-Bernoulli equation (2.1.4).

Chapter 3

Control

The ability to control dynamical systems is often desirable. The aim is to achieve a desired outcome for the system by applying certain inputs. These outcomes can take the form of specific configurations, trajectories, or other properties.

However, as systems get increasingly complex, determining the input to effectively control the system becomes more challenging. In fact, as we will see in our example, it might be directly counterintuitive. This is where optimal control theory is useful. It revolves around an objective function that is either minimized or maximized by a control input over time, while being subject to a set of constraints that govern the trajectory of the system [22], [23]. Additional constraints may also be present.

As the Chain of Pendulums model has proven feasible to model beams, it is now interesting to see if it can be utilized to determine input controls to obtain these desired properties when the system is subject to different conditions. To explore this, we consider the marine riser as a representative example.

3.1 Manual Control

We begin by investigating the effects of control forces on the system. In the motivating example of the marine riser system, our focus is on extending the longevity of the wellhead by reducing the *bending moment* at the seabed. Semi-submersible platforms maintain their position at sea through either mooring, essentially anchoring it to the seabed, or through automatic control using thrusters to counteract environmental and external forces [3]. We are now interested in exploring whether we can utilize these thrusters to also counteract the effects of the sea on the marine riser to reduce the bending moment. In general, we explore how we can manipulate a system to achieve desired outcomes by applying a control force at the end of the beam. The control force is denoted u, resulting in the Hamiltonian of the controlled Chain of Pendulums model

$$H(q,p) = \frac{1}{2}p^T M^{-1} p + \sum_{i=1}^{n}\sum_{k=1}^{n} F_k l_i e_3^T q_i + \sum_{i=1}^{n} u l_i e_3^T q_i + \frac{1}{2}\sum_{i=1}^{n} k_i \arccos^2(q_{i-1}^T q_i). \tag{3.1.1}$$

To analyze this scenario, we assume the marine riser is attached to the platform at the final node in such a way that it is not freely rotating in the yz-plane. This implies the presence of a certain stiffness in the connection, which we can represent by a spring in the endpoint. Therefore, we consider the Cantilever beam with a spring incorporated at the final node to account for the rigidity at the attachment point. As with the Fixed-Fixed beam, the spring constants in the attachment points are twice the spring constant of the rest of the system to represent the reacting moment. However, it is important to note that this setup differs from the Fixed-Fixed beam as the final node is not constrained and can be influenced by the system.

The bending moment is given by [24]

$$M(y) = EI\frac{d^2 z}{dy^2}(y).$$

As our model is discrete, we follow [18] and approximate the bending moment through finite differences

$$M_i = EI\frac{z_{i+1} - 2z_i + z_{i-1}}{l_{i-1}l_{i+1}}. \tag{3.1.2}$$

To express the bending moment at the origin, we require the displacement z_{-1} at the virtual node n_{-1}, which is spaced $l_{-1} = l_1$ from n_0. As this is a fixed boundary, the slope, the first order derivative of the deflection z_0, is zero [18]. This gives us the relation

$$\frac{dz}{dy} = \frac{z_1 - z_{-1}}{2l_1} = 0 \implies z_{-1} = z_1.$$

As the deflection in the origin is zero, we get the expression for the bending moment

$$M_0 = EI\frac{z_1 - 2z_0 - z_{-1}}{l_1^2} = EI\frac{2z_1}{l_1^2} = k_0\frac{2z_1}{l_1^2}, \tag{3.1.3}$$

where the spring constant k_1 is the spring constant of the first pendulum and considered equivalent to the flexural rigidity EI. However, as this constant only scales the expression, the specific value is not important when we aim to minimize the bending moment.

Now, as the control force is applied to the final node, it is straightforward to counteract an external force applied to the same node by letting the control force be of the same magnitude, but opposite direction, as the external force. The forces then cancel each other, resulting in no movement of the beam. However, as we restrict the control force to only be applied at the final node, it is of interest to explore how this force can be utilized to counteract external forces applied at other nodes.

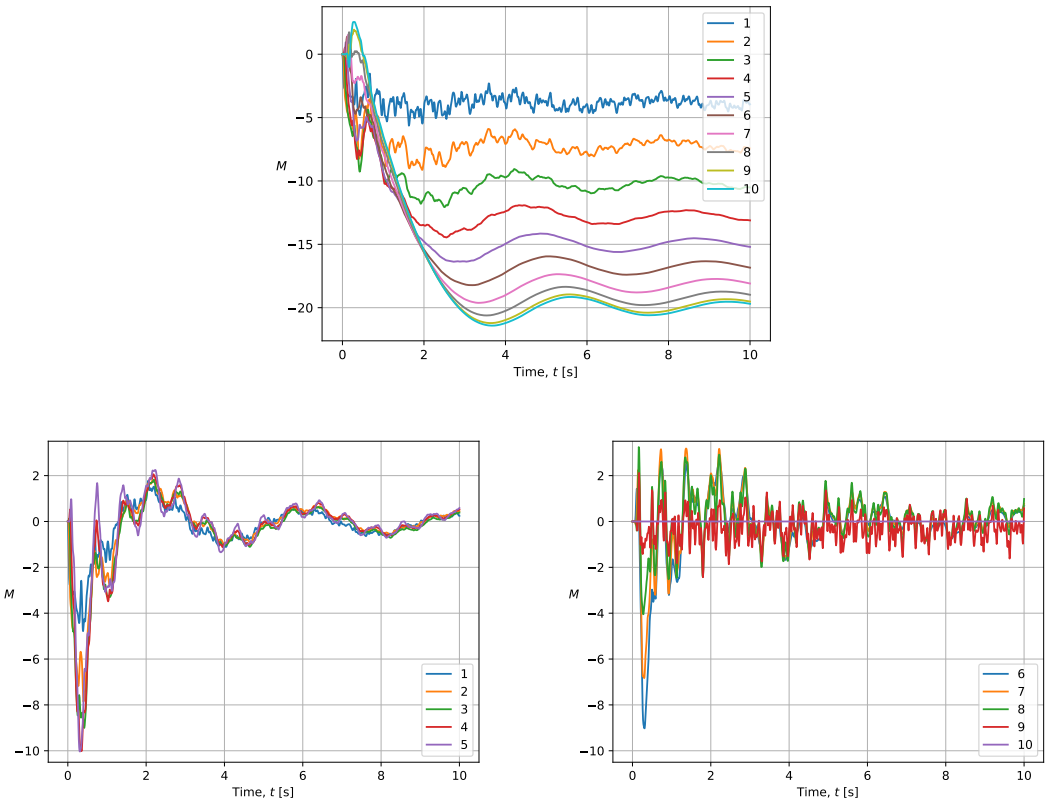

Figure 3.1: Evolution of the bending moment in the origin (3.1.3) of 10 different systems, with and without control force. External force $F = 2$ N is applied to node i in system i as shown in the legend. Top: No control. Bottom: Left: Controlled system 1-5. Right: Controlled system 6-10.

We consider the usual system consisting of $n = 10$ pendulums with lengths $l = 1$ m and mass $m = 1$ kg in the dissipative Chain of Pendulums model (2.4.4) with dissipation constant $D = 10$

kg/m. Ten different systems are considered, where the external force $F = 2$ N is applied to node i in system i. Figure 3.1 shows the evolution of the bending moment at node zero, with and without a control force. Animations of the systems can be found here. The top figure displays the bending moments of the uncontrolled systems, where it can be observed that the further the external force is applied from the origin, the greater its leverage is, resulting in a higher bending moment. By applying a control force to the final node, we can counteract the external force to a degree. The bottom plots of Figure 3.1 show the resulting bending moments when an external force is applied to node i and a control force is applied to the final node to counteract it. As expected, when the external force is applied to the final node, we can set the magnitude of the control force u to the same value and apply it in the opposite direction. The forces cancel each other as they are both applied to the same node, resulting in no bending moment. When the external force is applied to nodes other than the final node, we can see that the control forces are able to reduce the bending moment substantially, but not entirely.

The control forces u_i that result in the lowest average of absolute bending moment, $\sum_k^N |M_k|/N$, at the origin when an external force $F = 2$ N is applied to node i, were found to be $u = -$ [0.37 0.72 1.01 1.28 1.50 1.68 1.83 1.93 1.99 2] N. As the obtained control forces show, when the external force is applied further away from the origin, a higher force is needed to counteract it. Notice also that during the initial phase of the system, $t \in [0, 0.5]$, there is an inevitable bending moment. This might be because the external force is applied closer to the origin and affects it before the control force is able to counteract it. However, it has been demonstrated that by applying a control force at the final node, the bending moment at the origin can be partially reduced. This highlights the use of the dissipative Chain of Pendulums model (2.4.4) to feasibly simulate systems influenced by external forces and determine the necessary control forces to achieve desired effects.

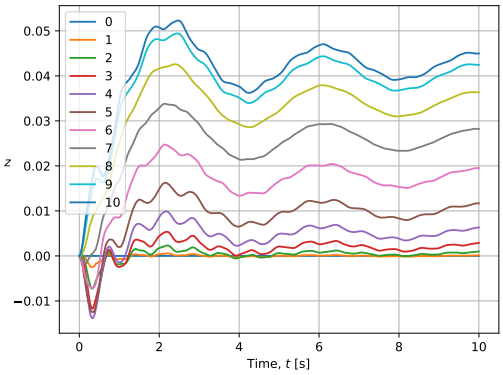

Figure 3.2: Trajectories of the nodes of the system where the external force $F = 2$ N is applied to the fifth node, and counteracted by the control force $u = -1.50$ N applied to the final node

To demonstrate the behavior of the systems, trajectories of the nodes of the system where the external force is applied to the central node is shown in Figure 3.2. Notice in particular that the control force moves the final node to oscillate around $z \approx 0.042$, this will be discussed and taken advantage of in the next section.

3.2 Constraints as a Reaction Force

In certain applications, it might be desirable to anchor or lock the position of the final node where the control force is applied. We think of it as a Fixed-Fixed beam where the final node can be unlocked, moved with a force, and then locked back in place. A practical example of this concept is the marine riser system. As observed in the system where the external force was applied to the fifth node in the last section, the control force that resulted in the most reduction of bending moment moved the final node to $z \approx 0.042$. The idea is then that if we are anticipating strong incoming currents, we can preemptively move and lock the position of the platform before the current arrives, counteracting the bending moment. This proactive action could potentially save energy, as it eliminates the need for continuous control forces. The necessary force applied would

only be the one needed to move the system into position.

In Section 2.4.1 constraints were introduced to restrict the movement of the final node in the z-direction. This works well for setting different beam support configurations. However, this approach becomes problematic if we want to apply a force to the locked node. To address this, the approach must be altered.

Notice how the term concerning this constraint in the dissipative Chain of Pendulums model of the Fixed-Fixed (2.4.2) and Pinned-Pinned (2.4.3) beams corresponds to a force λ_L acting on the final node. Consider differentiating the constraint in z-direction twice with respect to time in the system where also the dissipation is included

$$\begin{aligned}
0 &= \frac{dl}{dt}(q) = \sum_{i=1}^{n} l_i \dot{q}_i = l\left(\dot{q}\right) \\
0 &= \frac{d^2 l}{dt^2}(q) = \frac{dl}{dt}\left(\dot{q}\right) = l\left(\ddot{q}\right) = l\left(M^{-1}\dot{p}\right) = l\left(-M^{-1}\left(\frac{\partial H}{\partial q} - F_D(p) + \hat{G}(q)^T\hat{\lambda}\right)\right) \\
0 &= -LM^{-1}\frac{\partial H}{\partial q} - LM^{-1}G(q)^T\lambda - LM^{-1}L^T\lambda_l \\
\lambda_l(q,p,\lambda) &= -\frac{1}{LM^{-1}L^T}LM^{-1}\left(\frac{\partial H}{\partial q} - F_D(p) + G(q)^T\lambda\right),
\end{aligned} \tag{3.2.1}$$

where $LM^{-1}L^T$ is a scalar. Notice that $-\left(\frac{\partial H}{\partial q} - F_D(p) + G(q)^T\lambda\right)$ is the time differentiated conjugate momentum $\dot{p}$ of the dissipative Chain of Pendulums model (2.4.4) with only constraints in the pendulum lengths $g(q)$. By now adding this reaction force term as a force to the respective Hamiltonian we get

$$H^r(q,p) = \frac{1}{2}p^T M^{-1}p + \sum_{k=1}^{n} F_k \sum_{i=1}^{k} l_i e_3^T q_i + \lambda_l(q,p,\lambda)\sum_{i=1}^{n} l_i e_3^T q_i + \frac{1}{2}\sum_{i=1}^{n+1} k_i \arccos^2(q_{i-1}^T q_i),$$

where k_1 and k_{n+1} can be zero, depending on the type of boundary supports. By including dissipation, the resulting equations of motion are

$$\begin{aligned}
\dot{q} &= \frac{\partial H^r}{\partial p} = M^{-1}p \\
\dot{p} &= -\frac{\partial H^r}{\partial q} + F_D(p) - G(q)^T\lambda \\
&= \begin{bmatrix} k_1 s(q_0,q_1)q_0 + k_2 s(q_1,q_2)q_2 \\ k_2 s(q_1,q_2)q_1 + k_3 s(q_2,q_3)q_3 \\ \vdots \\ k_n s(q_{n-1},q_n)q_{n-1} + k_{n+1}s(q_n,q_{n+1})q_{n+1} \end{bmatrix} - \begin{bmatrix} \left(\sum_{k=1}^{n} F_k + \lambda_l(q,p,\lambda)\right) l_1 e_3 \\ \left(\sum_{k=2}^{n} F_k + \lambda_l(q,p,\lambda)\right) l_2 e_3 \\ \vdots \\ \left(F_n + \lambda_l(q,p,\lambda)\right) l_n e_3 \end{bmatrix} \\
&\quad - D\begin{bmatrix} p_1 \odot |p_1| \\ p_2 \odot |p_2| \\ \vdots \\ p_n \odot |p_n| \end{bmatrix} - \begin{bmatrix} \lambda_1 q_1 \\ \lambda_2 q_2 \\ \vdots \\ \lambda_n q_n \end{bmatrix},
\end{aligned} \tag{3.2.2}$$

which is an equivalent system to the supported beams (2.4.2) and (2.4.3), with dissipation. However, the final node is not locked in the z-coordinate and can thus later be influenced by control forces.

To illustrate this equivalence numerically, application of the two different approaches are shown in Figure 3.3 by applying them to the Fixed-Fixed and Pinned-Pinned beams, with dissipation constant $D = 0$. The solid lines represent the system with a constraint $l(q)$, while the dashed lines represent the system with the constraint replaced by a reaction force λ_l, showing equivalence.

Consider now the work of this reaction force λ_l. The constraint $l(q)$ restricted the movement of the final node in the z-axis. The reaction force λ_l achieves this by counteracting the forces from the system affecting the final node, ensuring that the acceleration of the final node in the z-direction is zero, $e_3^T\ddot{r}_n = 0$. As observed in Section 2.3, the acceleration of the final node is a function of $\dot{p}_n$, $\ddot{r}_n = \frac{\dot{p}_n}{m_n l_n}$. The reaction force λ_l is then causing the final equation of the dissipative

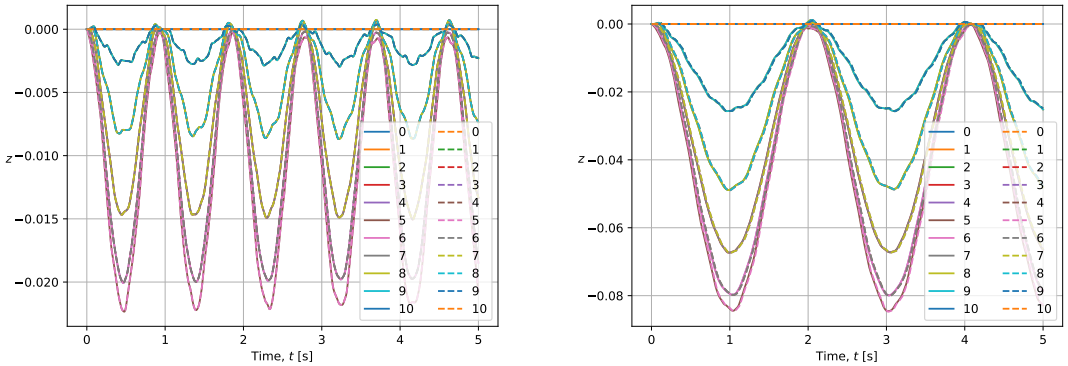

Figure 3.3: Trajectories of the nodes of the constrained beams modeled by the Chain of Pendulums model affected by a point load in the central node. The solid lines represent the system with a constraint (2.4.4), and the dashed lines represent the system where the constraint is replaced by a reaction force λ_l (3.2.2). Left: Fixed-Fixed beam. Right: Pinned-Pinned beam.

Chain of Pendulums model with constraint as a reaction force (3.2.2) to be $e_3^T \dot{p}_n = 0$. This causes the resulting acceleration from the system in this node to be zero. If we now apply a control force, that does not go into the expression of λ_l such that it is not counteracted, this force is the only term affecting the acceleration of the final node. This means that if we apply a force for some time and then remove it, the velocity of the node stays the same and continues in the same direction indefinitely.

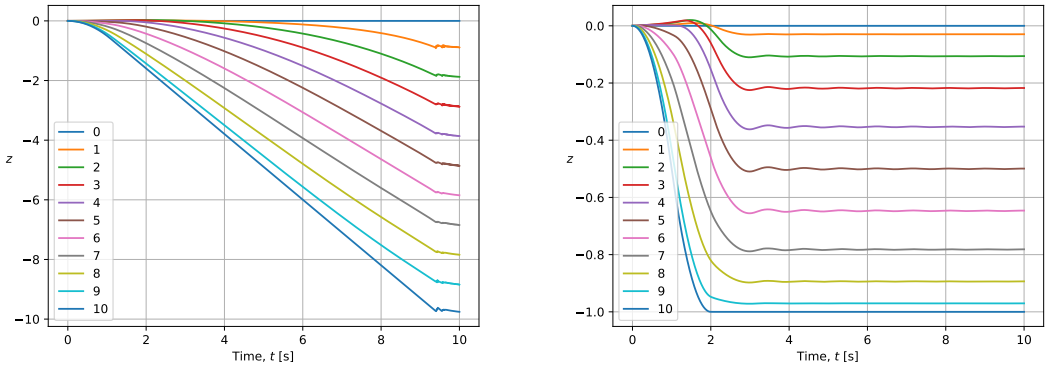

Figure 3.4: Trajectories of the nodes of the system modeled by the dissipative Chain of Pendulums model with the constraint as a reaction force (3.2.2). Left: Control force $u = 1$ N is applied over $t \in [0, 1]$. Right: Control force $u = 1$ N is applied over $t \in [0, 1]$ and then $u = -1$ N is applied over $t \in [1, 2]$.

This behavior is demonstrated in Figure 3.4(left) by showing trajectories of the nodes for the dissipative Chain of Pendulums model with constraint as a reaction force (3.2.2). No external forces are applied to the system, but we introduce a control force. In the left plot, control force $u = 1$ N is applied over $t \in [0, 1]$. As shown, even though the control force is applied only in the first second, there is nothing decelerating the node and eventually the system is infeasible as it approaches the total length of $L = 10$ m in the z-direction. A remedy to this is to apply an equal, but opposite force following it. Figure 3.4(right) shows this behavior where $u = 1$ N is applied over $t \in [0, 1]$ followed by $u = -1$ N over $t \in [1, 2]$, where the node stops and is stable.

Note that the actual force applied to perform this movement is now given by $\lambda_L + u$, where λ_L accounts for the system affecting the final node. This force can be seen in Figure 3.5(left). By now using this sum of forces $\lambda_L + u$ as an input into a simple dissipative Chain of Pendulums system (2.4.4) containing no z-constraint $l(q)$ or reaction force λ_L, we show the equivalence to the dissipative system with constraint as reaction force (3.2.2) in Figure 3.5(right), and animation of

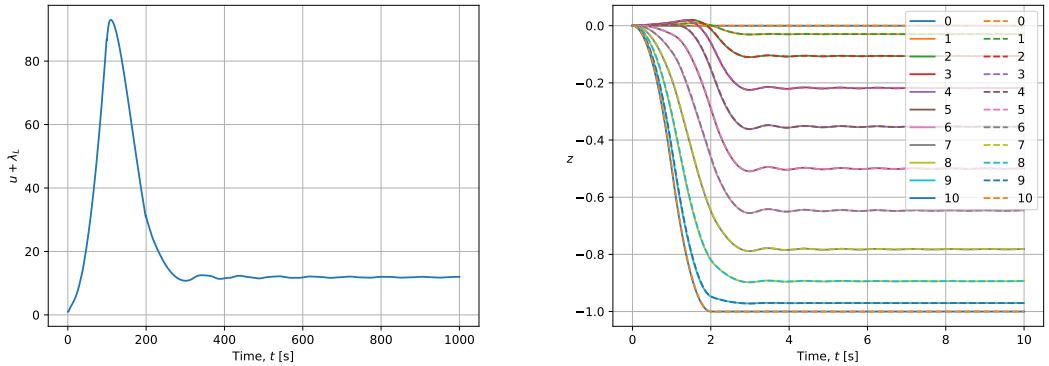

Figure 3.5: System affected by control force $u = 1$ N applied over $t \in [0, 1]$ and then $u = -1$ N is applied over $t \in [1, 2]$. Left: Input force necessary to achieve the trajectory shown in Figure 3.4(right). Right: Trajectories of the nodes of the constrained beams modeled by the dissipative Chain of Pendulums model with constraint in the z-axis as a reaction force (3.2.2), solid lines, compared to the dissipative model (2.4.4) with affected by a force that consist of $\lambda_L + u$, dashed lines.

the system can be found here. Thus, we can use the model (3.2.2) to determine the input force needed to obtain desired configurations. As the node becomes stationary at $t = 2$, a practical example of this in regards to the oil platform would be to apply the force in $t \in [0, 2]$, and then lock it in place mechanically such that it is not necessary to apply force in $t \in [2, 10]$.

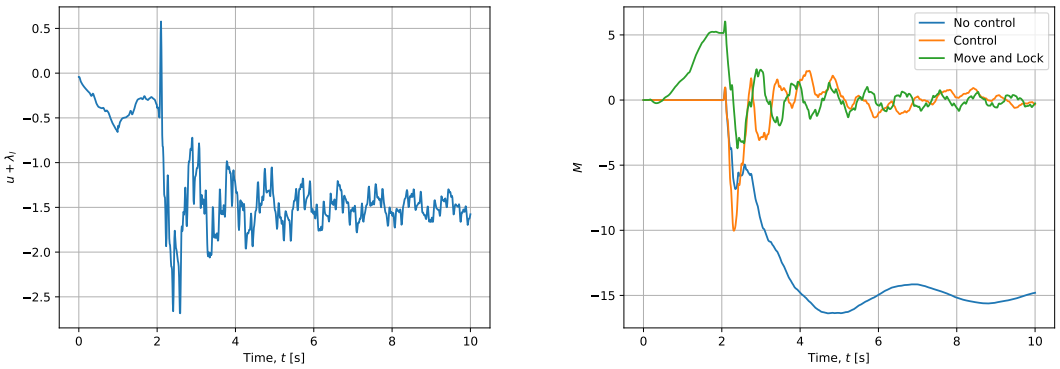

Figure 3.6: The system where an external force $F = 2$ N is applied to the central node at $t \in [2, 10]$. The system's final node is prior moved from $z = 0$ to $z = 0.042$ by a control force u. Left: Control force u. Right: Resulting bending moment of uncontrolled, control from last section, and the move and lock systems.

An application of this to reduce the bending moment is performed in Figure 3.6, and animation of the system can be found here. In this case, an incoming external force $F = 2$ N is applied to the central node in the time interval $t \in [2, 10]$. Prior to this, the node is moved from $z = 0$ to $z = 0.042$ by a force $u + \lambda_L$. Since the node can be anchored, the force in $t \in [0, 2]0$ is the only force required. Notice that the required force after oscillates around -1.5 N, as found in the previous section. The resulting bending moment is shown in Figure 3.6(right), where it is compared to the uncontrolled system and the system with a control force $u = -1.5$ N, as discussed previously. Both approaches effectively reduce the bending moment to oscillate around zero. Although the move and lock system initially causes a higher bending moment, it results in a smaller spike when the external force is applied. By locking the system at $t = 2$, we also observe that the required force force is lower in the move and lock system compared to the active control one, where the force $u = -1.5$ N is applied throughout the time. This shows the feasibility of the move and lock approach as a method to reduce the bending moment.

3.3 Optimal Control

In Section 3.1 it was shown that it is possible to control a dynamic system to achieve desirable outcomes by utilizing applying an input force. However, a trial and error approach as previously used can be slow, and might not even find the input that achieves the best outcome. This is accomplished by optimal control theory. The objective of optimal control theory is to find an admissable control u^* that causes the system governed by

$$\dot{x}(t) = f(x(t), u(t), t)$$

to follow an admissable trajectory x^* that minimizes the performance measure [22]

$$J = J_T(x(t_f), t_f) + \int_{t_0}^{t_f} J_R(x(t), u(t), t)dt. \tag{3.3.1}$$

The control u^* and the trajectory x^* are then considered optimal [22]. As the measure J is typically minimized, it is often viewed as a cost. The general form of the optimal control problem is then

$$\begin{aligned} \min_{u} \quad & c_T(x(t_f), t_f) + \int_{t_0}^{t_f} c_R(x(t), u(t), t)dt \\ \textbf{subject to } & \dot{x}(t) = f(x(t), u(t), t) \\ & x(t_0) = x_0 \\ & t \in [t_0, t_f], \end{aligned}$$

where the cost function is split into the *terminal cost* and the *running cost*. The terminal cost is a function of the final state $x(t_f)$, while the running cost includes the costs of the intermediate states $x(t)$ and controls $u(t)$ for $t \in [t_0, t_f]$. Considering a discrete-time, the problem can be reformulated as [23]

$$\begin{aligned} \min_{u} \quad & c_T(x_N) + \sum_{k=0}^{N} c_R(x_k, u_k) \\ \textbf{subject to } & x_{k+1} = f_k(x_k, u_k) \quad \text{for } k = 0, \ldots, N. \end{aligned}$$

Various methods exist to solve optimal control problems. The choice of method depends on the characteristics of the specific system. In our case, the system is discrete, nonlinear, implicit, high-dimensional, and imposes additional constraints at each time step. At every time step, a set of the RATTLE equations (1.6.1) is implemented, where $p_{n+1/2}$ is an intermediate equation inserted into the others. The variables involved in each step have dimensions as $q \in \mathbb{R}^{3n}$, $p \in \mathbb{R}^{3n}$, $\lambda \in \mathbb{R}^n$, and $\mu \in \mathbb{R}^n$. Thus, each time step establishes $3n + 3n + n + n = 8n$ constraint equations, amounting to $8Nn$ constraint equations when considering N time steps. The addition of a control force per time step increases the amount of variables by N. Since the system of $n = 10$ pendulums correlated well with the beams, we consider the same discretization here. As previously shown, a force applied to to the final node does not affect the first few nodes until several time steps have passed, as the movement propagates towards the origin. Thus, we consider $N = 10$ time steps, with a stepsize of $h = 0.01$. This means we are dealing with 800 constraint equations, involving 800 state variables and 1-10 control variables. Through experiments, it has been determined that global solvers are impractical for this configuration, and local solvers are preferred.

Sequential Quadratic Programming is a highly effective approach for solving nonlinear constrained optimization problems [25]. A local solver employing this method is the Sequential Least SQuares Programming (SLSQP), which is supplied by Python's scipy library. SLSQP, originally developed by Dieter Kraft [26] is a local minimizer capable of handling nonlinear terms and constraints. The algorithm follows a sequential quadratic programming approach to solve nonlinear constrained optimization problems of the form

$$\begin{aligned} \min_{x \in \mathbb{R}^n} \quad & f(x) \\ \textbf{subject to } & g_i(x) = 0, \quad i = 1, \ldots, m \\ & h_j(x) \geq 0, \quad j = 1, \ldots, p \end{aligned}$$

to a local minimum. The problem is solved iteratively by the steps

$$x_{k+1} = x_k + \alpha_k d_k,$$

where d_k is the search direction and α^k the stepsize. The search direction is determined by considering a quadratic programming subproblem, formulated by a quadriatic approximation of the Lagrangian of the problem

$$L(x, \lambda, \mu) = f(x) - \lambda g(x) - \mu h(x),$$

along with a linear approximation of the constraints $g(x)$ and $h(x)$. This subproblem takes the form of a typical quadratic programming problem

$$\begin{aligned} \min_{d \in \mathbb{R}^n} \quad & \frac{1}{2} d^T \nabla^2_{xx} L(x_k, \lambda_k, \mu_k) d + \nabla f(x_k)^T d \\ \textbf{subject to} \quad & \nabla g_i(x_k)^T d + g_i(x_k) = 0, \quad i = 1, \dots, m \\ & \nabla h_j(x_k)^T d + h_j(x_k) \geq 0, \quad j = 1, \dots, p, \end{aligned}$$

which can be solved by various quadratic solvers [26]. In the implementation of SLSQP, it is solved by a nonlinear least-squares solver, hence the name of the method.

3.3.1 Numerical Experiments

Let $\tilde{Y}$ be the output of the optimizer. The system is comprised of N time steps, where each time step k consists of the configuration $Y_k = \begin{bmatrix} q_k^T & p_k^T & \lambda_k^T & \mu_k^T \end{bmatrix}^T$. Note that subscript here represents the current time step. Thus, the output $\tilde{Y}$ includes these configurations as well as the input control $u = \begin{bmatrix} u_0 & \dots & u_N \end{bmatrix}$, resulting in $\tilde{Y} = \begin{bmatrix} Y_0^T & \dots & Y_N^T & u^T \end{bmatrix}^T$.

Following the approach in Section 3.1, we consider the Cantilever beam including a spring in the final node to represent the marine riser. The same parameter values are used, with pendulum lengths of $l = 1$ m, and masses $m = 1$ kg. We explore four different cases.

1. Minimize the bending moment at the final time $t = T$ by optimizing the control force u applied to the final node, which remains constant throughout each time step t_0 to t_N.
2. Minimize the bending moment at every time step by optimizing the control force u applied to the final node, which remains constant throughout each time step t_0 to t_N.
3. Minimize the bending moment in the final time $t = T$ by optimizing the control force u applied to the final node, which can vary in time $u = \begin{bmatrix} u_0 & \dots & u_N \end{bmatrix}^T$.
4. Minimize the bending moment at every time step by optimizing the control force u applied to the final node, which can vary in time $u = \begin{bmatrix} u_0 & \dots & u_N \end{bmatrix}^T$.

In each case, we consider ten systems where an external force $F = 2$ N is applied to node i in system i.

Minimize Final Bending Moment

First, we consider the system where an external force is applied to the final node. As before, to control the system, a constant control force $u_0 = \cdots = u_N = u$ is also applied to the final node. The property we want to control is the bending moment in the final step $t = T$. In order to establish an appropriate objective function, we square the bending moment (3.1.3) to create a function with a minimum. Thus, our objective function is

$$c(\tilde{Y}) = \left(2k_1 \frac{z_1^{(T)}}{l_1^2} \right)^2, \tag{3.3.2}$$

where $z_1^{(T)}$ is the z-component of the first pendulum at time $t = T$.

Let the q-components of the initial guess $\tilde{Y}_0$ be $q_i^{(k)} = \begin{bmatrix} 0 & 1 & 0 \end{bmatrix}$ for $i = 1, \dots, n$, and time steps $k = 0, \dots, N$, while the remaining components are zero. The initial guess corresponds

to a horizontal beam configuration at every time step. The motivation behind this choice is to encourage the resulting trajectory to remain close to the original configuration to reduce the amount of bending moment and control input needed. As a reference, we run the system without a control force u. This results in an objective function of $c(\tilde{Y}) = 1.0843 \times 10^3$ N^{2}m^2.

Next, we implement the control force u and optimize over it to minimize the objective function. The resulting objective function value is $c(\tilde{Y}) = 3.9027 \times 10^{-4}$ N^{2}m^2, where the optimal control force is found to be $u = -0.4301$ N. However, as the external force is applied to the final node, we know from Section 3.1 that applying a control force of the same magnitude in the opposite direction would cancel it out, resulting in $c(\tilde{Y}) = 0$. Therefore, this solution is not a global solution, but a local one.

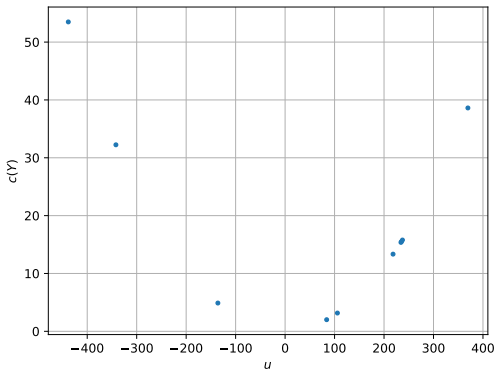

Figure 3.7: Objective function $c_{\text{sum}}(\tilde{Y})$ of ten randomized initial conditions of the Cantilever beam with a spring in the final node, affected by an external force $F = 2$ N in the final node. Every point is a local solution of the optimizer.

As local solvers depend on the initial guess, it is of interest to explore different initial guesses. Thus, we apply the optimization to ten different random initial guesses, each of the form $\tilde{Y}_0 + U(-0.1, 0.1)$, where $\tilde{Y}_0$ is the horizontal beam at every time step as previously described. The resulting objective function values are shown as a function of the optimal control force in Figure 3.7. Each point is a solution given from the optimizer, meaning there are several local optima the local solver converged to. As observed, the slightest variations in the initial guess results in vastly different solutions. However, the shape resembles a parabola, indicating the presence of a global minimum. This aligns well with our assumption that the optimal control force is $u = -2$ N, as the parabola seems to have a minimum around that value.

To search for the global minimum, one approach could involve running the local solver with numerous random initializations, followed by performing regression analysis to identify the underlying function. However, it is worth noting that applying the local solver on random initial data has been found to be computationally expensive. Moreover, an initial guess closer to a previous solution allows for a faster convergence to a new solution. Furthermore, as the solution space in regards to u is seemingly convex, an alternative strategy is adopted that utilizes a gradient-based stepping algorithm.

The concept involves using the result of a local solve to update the control force, guided by the derivative of the objective function. The updated result is then used as the initial guess for subsequent optimizations. This iterative approach facilitates a step-by-step refinement process, progressively improving the solution by adjusting the initial guess based on the result and the derivative of the objective function obtained from the previous solve.

Let $\tilde{Y}_m$ represent the solution obtained from the mth local optimization. To update the control force u for the subsequent local optimization, we consider the derivative of the objective function using backward differences. The update equation for u is given by

$$u_{\text{next}} = u_m + \alpha \frac{c(\tilde{Y}_m) - c(\tilde{Y}_{m-1})}{u_m - u_{m-1}}, \tag{3.3.3}$$

where α denotes the step size. The algorithm proceeds as follows

1. Perform a local optimization using $\tilde{Y}_0$ as the initial guess.
2. Perform another local optimization using the result from the first solve as the new initial guess, where the guess for u is perturbed.
3. Calculate u_{next} using the update equation (3.3.3).
4. Perform a local optimization with $\tilde{Y}_{\text{next}} = \begin{bmatrix} \tilde{Y}_{m,0}^T & \dots & \tilde{Y}_{m,N}^T & u_{\text{next}}^T \end{bmatrix}^T$ as the initial guess, where $\tilde{Y}_{m,k}$ represents the components at time step k of solution m.
5. Repeat steps 3 and 4 unless $|c(\tilde{Y}_m) - c(\tilde{Y}_{m-1})| < \text{tol}$.

This iterative procedure continues until the improvement in objective function between consecutive iterations falls below the specified tolerance, indicating convergence.

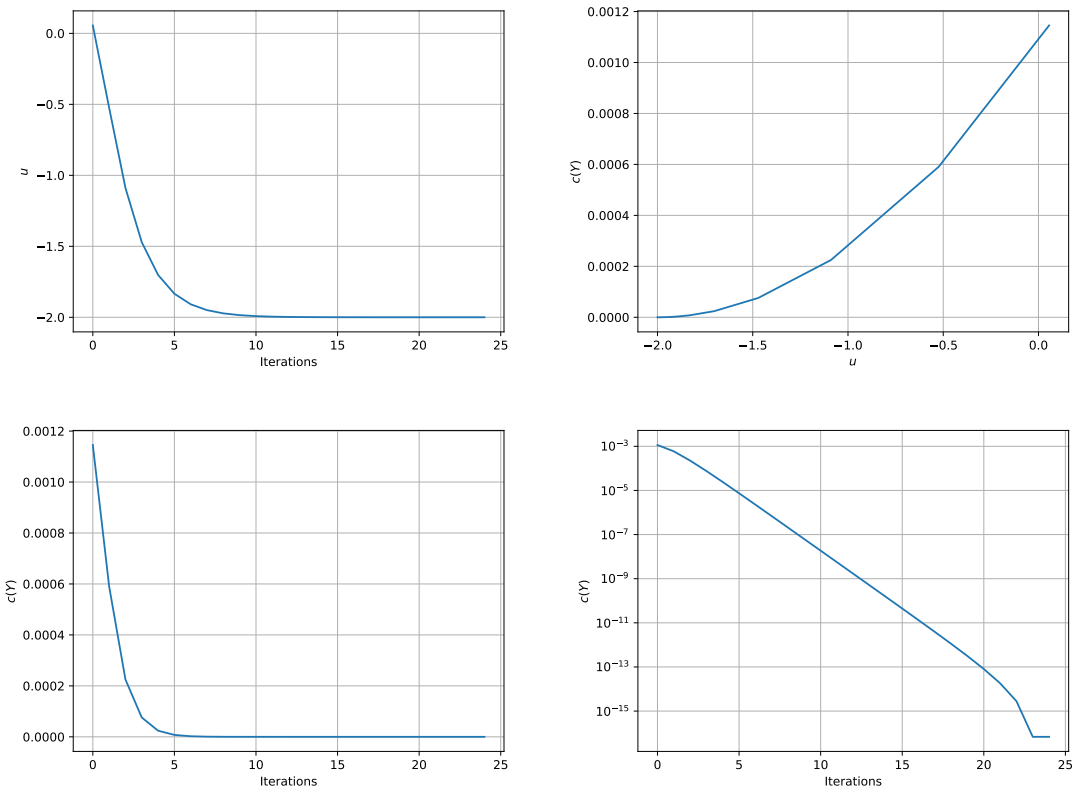

Figure 3.8: Optimization results of the Cantilever beam with spring in the final node, affected by an external force $F = 2$ N in the final node. Left row shows the evolution of the control force u and the resulting objective function $c(Y)$. Top right: figure shows the objective function $c(Y)$ against the control force u. Bottom right: log plot of the objective function.

We apply the algorithm to the same system where an external force is applied to the final node. The results of the optimization are shown in Figure 3.8. The top-left figure demonstrates the convergence of the control force u towards -2, while the bottom figures show the convergence of the objective function towards 0, aligning with our expectations. As anticipated, plotting the objective function $c(\tilde{Y})$ against the control force u reveals a parabolic shape, as shown in the top-right plot. The optimal control force obtained is $u = -2.00000082$ N, resulting in an objective function value of $c(Y) = 6.9699 \times 10^{-16}$ N^{2}m^2.

Constant Control Force, Final Bending Moment

With the algorithm established, we apply it to the remaining systems where the external force $F = 2$ N is applied to the ith node in system i. The optimal control force u and the resulting

objective function $c(\tilde{Y})$ is found for each system and shown in Table 3.1. Animations can be found here. As the results show, there exist optimal forces that reduce the objective function to an order of 10^{-16} or even lower for every system. However, some interesting observations can be made.

Table 3.1: Constant optimal control force u applied to the final node and resulting objective function $c(\tilde{Y})$ of the Cantilever beam with a spring in the final node affected by a force $F = 2$ N at node i.

Node	u [N]	$c(\tilde{Y})$ $[\mathrm{N}^2\mathrm{m}^2]$
1	189.36479384	1.6088×10^{-18}
2	265.06121792	1.9193×10^{-18}
3	233.73855219	1.4145×10^{-17}
4	131.92079771	8.1984×10^{-18}
5	-33.40695642	1.3053×10^{-16}
6	-78.44287539	9.5851×10^{-16}
7	-5.83282449	2.8146×10^{-16}
8	16.25442723	4.0766×10^{-18}
9	1.30856873	5.0050×10^{-16}
10	-2.00000082	8.1400×10^{-16}

When the external force is applied to certain nodes, particularly nodes 1-4, 8, and 9, the optimal force is in the same direction as the external force. In Section 3.1 we considered the average of the absolute bending moment, which resulted in every control force being in the opposite direction of the external force. This is reasonable, as it was necessary to consider the bending moment at the entire time over a longer period. Thus, if a control force is added in the same direction as the external force, it increases the bending moment in the long term.

Now consider the optimal control. The bending moment is still evaluated as the squared z-value of the initial pendulum. However, as we are now only concerned by the bending moment in the final time $t = T$, the optimal control seeks to obtain a configuration where the initial pendulum is horizontal at time $t = T$. To understand how a control force in the same direction as the external force can achieve this, we examine the system where the external force $F = 2$ N is applied to the fourth node, along with the optimal control force found applied to the final node. The trajectory of the beam is shown in Figure 3.9(left), and animation of the system is available here. It can be observed that when an arbitrary force is applied to a beam, there exists an initial proportional backward propagating wave in the nodes, causing the nodes to move in the opposite direction relative to the applied force. This wave counteracts the effect of the external force, reducing the bending moment at the final time $t = T$.

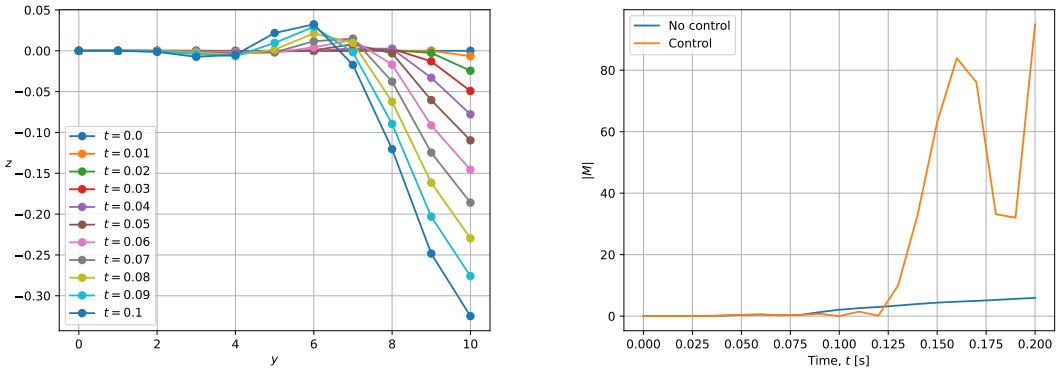

Figure 3.9: Left: Trajectory of the Cantilever beam with spring in the final node, affected by an external force $F = 2$ N in the fourth node , and a control force at the final node as usual. Left: Trajectory. Right: Absolute bending moment of the same Cantilever beam affected by the obtained optimal control force $u = 131.92079771$ N over time $t \in [0, 2T]$, to show increased bending moment. A reference system with no control $u = 0$ is also plotted.

An optimal control force aligned with the external force is a result of the limited number of time steps. If we were to increase N and apply the same force, it would naturally result in a higher bending moment as the added force induces a greater deflection in the beam. To demonstrate this, we apply the obtained optimal control force $u = 131.92079771$ N over twice the time $t \in [0, 2T]$ and compare it to the system without a control force. This is shown in Figure 3.9(right). Although the objective function is minimized at $t = 0.1$, the magnitude of the bending moment increases in the following time. This confirms that a higher control force leads to an increased bending moment over time.

As the external force is applied closer to the first node, the magnitude of the necessary control force becomes significantly higher. This may be attributed to the fact that a stronger backpropagating wave is necessary to counteract the influence of the external force. The closer the force is to the first node, the earlier it begins affecting it, accumulating a higher overall effect, requiring a higher control force to counteract it. However, the reason for the lower magnitude when the external force is applied to the first node remains unclear.

The control force necessary to counteract the external force $F = 2$ N close to the first node is over two orders of magnitude higher than the external force itself. This seems excessive, and as illustrated in Figure 3.9(right) a high control force leads to increased bending moment over time. This might not be a desired result in the context of a system like the marine riser that seeks to minimize the overall bending moment.

Constant Control Force, Sum of Bending Moment

In Section 3.1 systems over the time interval $t \in [0, 10]$ were considered and optimal control forces were obtained through trial and error. These control forces were of the same magnitude as the external force $F = 2$ N. However, as explored in the previous section, when minimizing the bending moment in the final time $t = T$, the effect of the control force on the bending moment in other time steps is neglected. To attempt to address this, we reformulate the objective function to account for every time step $k = 0, \ldots, N$ as

$$c_{sum}(\tilde{Y}) = \sum_{k=0}^{N} \left(2k_1 \frac{z_1^{(k)}}{l_1^2} \right)^2 . \tag{3.3.4}$$

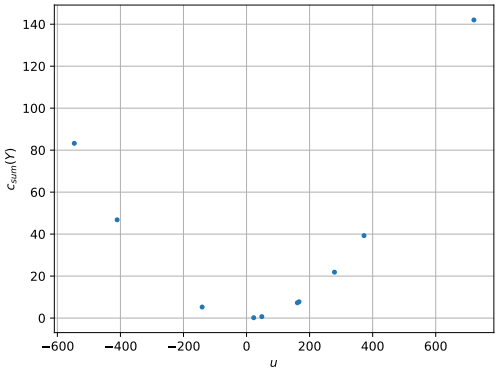

Figure 3.10: Objective function $c_{\text{sum}}(\tilde{Y})$ of ten randomized initial conditions of the Cantilever beam with a spring in the final node, affected by an external force $F = 2$N in the final node. Every point is a local solution of the optimizer.

To examine the landscape of the solution space, we follow the same approach as in the previous section and explore the relationship between the control force u and the objective function $c_{\text{sum}}(\tilde{Y})$ for the system where the external force $F = 2$ N is applied to the final node. Figure 3.10 shows this relation, where it again resembles a parabolic shape. This suggests a global minimum, and we proceed with the same algorithm as before.

The approach is applied to the ten different systems where the external force $F = 2$ N is applied to node i in system i. The results are presented in Table 3.2 and animations of the systems

Table 3.2: Optimal control force u applied to the final node and resulting objective function $c_{\text{sum}}(\tilde{Y})$ of the Cantilever beam with a spring in the final node affected by a force $F = 2$ N at node i.

Node	u [N]	$c_{\text{sum}}(\tilde{Y})$ $[\text{N}^2\text{m}^2]$
1	246.22516042	4.8718×10^{1}
2	333.81910050	5.4252×10^{1}
3	274.01518234	2.0801×10^{1}
4	144.46879653	1.1853×10^{0}
5	-47.56869973	2.0774×10^{0}
6	-84.88904775	1.9489×10^{-1}
7	-3.11411524	4.9376×10^{-2}
8	17.00748153	2.3867×10^{-3}
9	0.96230324	5.5586×10^{-5}
10	-2.00000132	6.8049×10^{-16}

can be found here. When the external force is applied to the final node we obtain a solution of the same order as with the objective function concerned with the final bending moment. The optimal control force is obtained by applying a force of equal magnitude in the opposite direction, canceling out the external force. However, for external forces applied to other nodes, the control force is not able to reduce the sum of squared bending moments to the degree of the final bending moment in the previous section. The resulting objective function is increasingly higher as the external force is applied closer to the first node, but for the first node itself. However, notice that the resulting optimal forces obtained are similar to the ones found for the final bending moment.

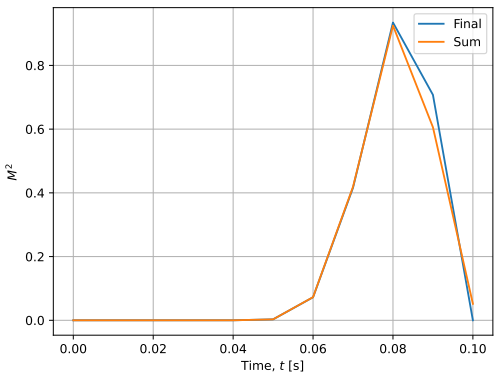

Figure 3.11: Squared bending moment of the Cantilever beam with a spring in the final node, affected by an external force $F = 2$ N in the fifth node. Final: System affected by the control force obtained by optimizing the final squared bending moment. Sum: System affected by the control force obtained by optimizing the sum of squared bending moments.

We investigate further by examining the squared bending moment over time of the two systems where the external force is applied to the fifth node. The resulting squared bending moments are shown in Figure 3.11. The system minimizing the bending moment in the final time $t = T$ achieves a lower bending moment at that specific time. On the other hand, the system minimizing the sum of bending moments sacrifices the bending moment at the final time to obtain an overall lower sum of bending moment. The sum of squared bending moment in the system minimizing the bending moment at the final time is 2.1335 N^2m^2, while for the system minimizing the sum it is 2.0774 N^2m^2. In an uncontrolled beam the bending moment increases over time until the beam reaches its maximum deflection and begins to return. As our simulation does not extend this far in time, the maximum bending moment in an uncontrolled system is reached at the final time $t = T$. Consequently, optimizing the bending moment at this time leads to the greatest reduction in overall bending moment as well, explaining the similar optimal control forces obtained between the systems with the two different objective functions.

Furthermore, this explains why the obtained control forces here are also of a significantly

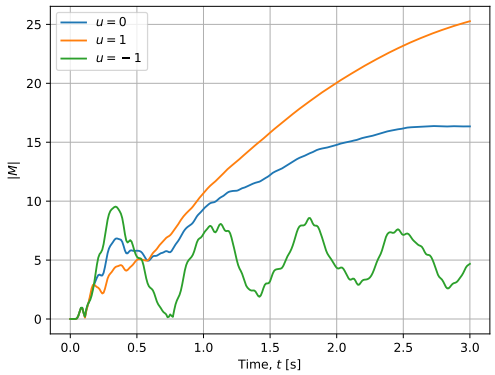

Figure 3.12: Absolute bending moment of the Cantilever beam with a spring in the final node, affected by an external force $F = 2$ N in the fifth node. The system is simulated three times, with $u = 0, 1, -1$ N.

higher magnitude than the manual control forces found for the system with a longer timeframe. As previously observed in Figure 3.9(right), the strong force results in a lower bending moment in the short term, but higher in the long term. To also illustrate the impact of the sign of the control force, we consider the same system affected by the external force $F = 2$ N in the fifth node. The system is simulated three times; without a control force, with $u = 1$ N, and with $u = -1$ N. The resulting absolute bending moment is shown in Figure 3.12. As observed, applying a control force in the same direction as the external force might reduce the bending moment initially, but leads to an increase in the long term. Conversely, by applying a control of opposite sign, the system exhibits the opposite effect, while it might increase the bending moment in the beginning, it is reduced in the long term. To obtain similar results in the optimization, it is necessary to extend the timeframe, making the system increasingly computational expensive. This is left for future work. Nonetheless, our results demonstrate that within a time interval $t \in [0, T]$, it is possible to minimize both the final bending moment and the sum of bending moments through optimization.

Variable Control Force

In the previous sections, the systems are optimized over a constant control force u. However, we now let the control force vary with time, i.e. $u = \begin{bmatrix} u_0 & \dots & u_N \end{bmatrix}$. Note that the control force u_N is only applied at $t = T$, thus it is only a part of the equation for the conjugate moment at the final time p_T and does not affect the configuration of the pendulums, and thus not the bending moment.

Due to the nature of the equations, the control forces at each time step are not independent of each other. This means that one value of u_i does not result in one value of the objective function $c(\tilde{Y})$ as it also depends on the other control forces u_j, $j \neq i$. Therefore, the solution space becomes more complex compared to the case of the constant control force. To illustrate this, the system affected by an external force in the final node is optimized over ten different random guesses. The resulting control forces u_i are plotted against the objective function $c(\tilde{Y})$ in Figure 3.13(left). Each horizontal line of points represents a local solution of the optimizer, $u = \begin{bmatrix} u_0 & \dots & u_N \end{bmatrix}$.

As the solution space with regard to u has a dimension of $N + 1$ it is challenging to visualize it properly. However, as we know the optimal force for the system where the external force is applied to the final node, we can investigate the solution space further by carefully choosing the initial guesses. As an intitial guess, we use the horizontal beam at every time step, $\tilde{Y}_0$, as used for the constant control force. We perform 21 simulations, where the control force $u \in \mathbb{R}^{N+1}$ is initialized with values ranging from -10 in the first simulation to 10 in the final simulation. As observed in Figure 3.13(right), the relation between the control force u and objective function $c(\tilde{Y})$ is nonconvex. However, as the solution space contains minima, and we observe that the minimum achieved in the constant control case is contained in this space. Thus, we apply the same approach as used for the constant control force and investigate the results.

Applied to the objective function concerned with the final bending moment $c(\tilde{Y})$ (3.3.2) we

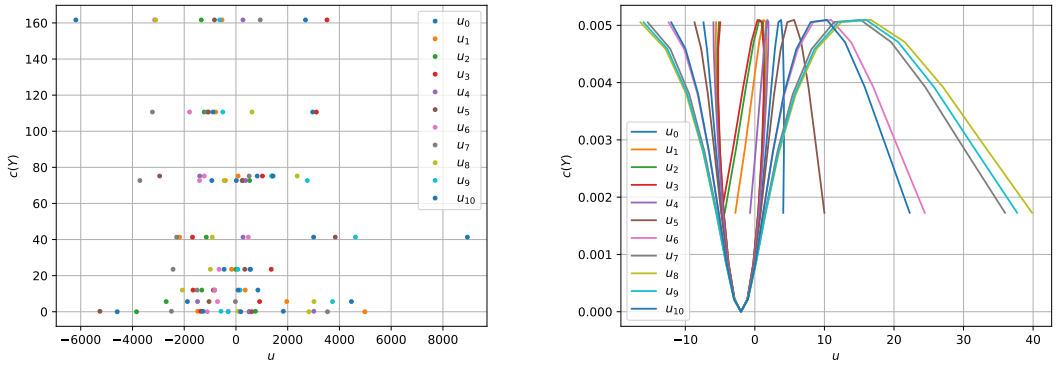

Figure 3.13: Objective function $c(\tilde{Y})$ of different initial conditions of the Cantilever beam with a spring in the final node affected by an external force $F = 2$ N in the final node. Left: Ten randomized initial conditions. Every horizontal line of points is a local solution of the optimizer, $u = \begin{bmatrix} u_0 & \dots & u_N \end{bmatrix}$. Right: Solutions of 21 initial conditions of the form $\tilde{Y}_0$, with the control forces u initialized as a vector of -10 in the first simulation, up to 10 in the final.

get the results shown in Table 3.3, with animations of the systems found here. Comparing them to the results obtained with the constant control force, we observe that the values of the objective functions are quite similar. In fact, when considering the initial force u_0 in every simulation, they correlate well with the forces obtained when using the constant control force, following the same behavior. However, in every simulation but the one where the external force is applied to node 8, the magnitude of the initial control force is higher than that in the case of the constant control force. This is compensated by the control forces in the subsequent time steps, where the magnitudes are lower, even to the point that the forces are applied in the opposite direction. Conversely, when the external force is applied to node 8, where the magnitude of the initial force is lower, it results in a necessary increase of magnitude in the subsequent control forces to compensate.

Applied to the objective function concerned with the sum of bending moment $c_{\text{sum}}(\tilde{Y})$ (3.3.4) we get the results shown in Table 3.4, with corresponding animations shown here. As we know the solution space is nonconvex and the method relies on gradient-based stepping, the solutions are not necessarily global solutions. Notably, this is exhibited in the systems 9 and 10, where the objective functions are higher than in the constant control force case. However, in the other systems the resulting objective functions are lower. The forces in system 6, 7, and 8 exhibit the same behavior as in the control of the final bending moment. They overshoot the initial force and compensate with the subsequent ones. The remaining initial forces, except for system 9, also show similarities to the final bending moment case, but with vastly higher magnitude. This leads to subsequent forces that follow no specific pattern, but still seem to compensate as nice results are achieved. Similar to the constant control case, as the external force is applied closer to the first node there seems to be an inevitable bending moment that the optimal control is unable to counteract. However, as the majority of the objective functions are found to be lower in the variable control force case, this indicates that a varying control force can be beneficial.

A common characteristic observed in all four applications is that the required force is often significantly higher than the external force. As we have investigated, in the long term the optimal control forces are likely more in line with the external force, as well as of the opposite sign. Further, while the results of the optimization method applied to the system with variable control forces are generally superior to those with a constant control force, it is important to note that they may not necessarily be global minima. Thus, the method needs to be refined or alternative approaches are required to obtain the optimal solutions. This could not be addressed here because of lack of time, but could be an interesting idea to further develop this work in the future. However, the Chain of Pendulums model (2.4.4) has been shown to be a feasible model to simulate a beam subjected to an external force. Furthermore, when control forces are introduced, the model has shown to be a useful tool to obtain the forces that result in the desired configurations, here demonstrated by the minimization of the bending moment.

Table 3.3: Optimal control force u [N] that can vary with time applied to the final node and resulting objective function $c(\tilde{Y})$ $\left[\mathrm{N}^2\mathrm{m}^2\right]$ of the Cantilever beam with spring in the final node affected by a force $F = 2$ N at node i. Each column is the optimal control force u applied to the final node, when the external force is applied at the labeled node. The unit of the time is seconds [s].

Time \ Node	1	2	3	4	5
0.00	236.74133327	336.07846291	289.84494113	144.18617042	-40.90733296
0.01	176.03657742	248.30055387	220.07943386	122.74419855	-30.90733825
0.02	-91.13385252	-119.18838543	-125.61824705	71.61596737	16.03757973
0.03	-148.34963289	-194.08371464	-195.67926663	59.86414075	26.78916708
0.04	-147.06883776	-196.80056785	-196.02032353	60.84293522	26.12691278
0.05	-142.63256952	-191.26978514	-185.95669073	60.84854218	25.52924716
0.06	-138.73639081	-180.80492541	-174.42478643	58.98999427	25.59134617
0.07	-139.94686635	-183.23009601	-178.32198956	59.48248966	25.69001347
0.08	-139.67629721	-182.20331876	-180.31818323	63.34127417	25.79474109
0.09	-145.28923069	-192.55433848	-191.93230369	69.24579499	25.93698519
0.10	-150.40062866	-205.89133479	-209.32601373	76.62785812	26.10258524
$c(\tilde{Y})$	4.0945×10^{-17}	2.5435×10^{-17}	3.9247×10^{-16}	1.8344×10^{-15}	4.5781×10^{-17}
Time \ Node	6	7	8	9	10
0.00	-95.46210526	-6.37676723	15.98768258	1.64128235	-1.98358725
0.01	-72.55977186	-5.59399816	16.16410765	1.16735236	-2.01967044
0.02	36.03612105	-2.52496485	19.58818894	-0.74587108	-1.99445916
0.03	60.54844304	-1.86365698	20.41864921	-1.17006398	-1.98511074
0.04	58.96439362	-1.97369357	20.41717481	-1.12772405	-1.97221356
0.05	57.39323004	-2.07293974	20.39390366	-1.09354455	-1.94501753
0.06	57.16056724	-2.10357742	20.41158897	-1.08836304	-1.90881344
0.07	57.51978053	-2.10814051	20.48247445	-1.08205005	-1.87815492
0.08	58.09627268	-2.09988998	20.65043704	-1.07378366	-1.86172179
0.09	58.98919866	-2.09408005	20.87561786	-1.06406104	-1.85233172
0.10	60.13246326	-2.08584044	21.20639103	-1.04496325	-1.88918937
$c(\tilde{Y})$	9.9845×10^{-18}	3.0662×10^{-17}	1.1204×10^{-16}	2.9744×10^{-17}	1.6018×10^{-15}

Table 3.4: Optimal control force u [N] that can vary with time applied to the final node and objective function $c_{\text{sum}}(\tilde{Y})$ $\left[\text{N}^2\text{m}^2\right]$ of the Cantilever beam with spring in the final node affected by a force $F = 2$ N at node i. Each column is the optimal control force u applied to the final node, when the external force is applied at the labeled node. The unit of the time is seconds [s].

Time \ Node	1	2	3	4	5
0.00	594.81474357	734.53746131	1475.94727906	352.56992367	-316.89492696
0.01	-164.82820687	-66.39640948	-1109.32694312	-92.41837026	267.77956396
0.02	-144.79824977	-325.44084065	-451.13303263	-96.47953678	123.66056989
0.03	-106.62225278	578.00391891	525.14603558	-103.46457461	99.14706291
0.04	-103.90817214	-9.55167963	-16.92310237	-160.77945464	-57.76137233
0.05	11.32011214	-1508.58534423	-25.32316335	-78.70051674	-104.87930687
0.06	18.98567128	344.26286117	180.90411028	405.61715537	-78.02650546
0.07	-104.51233325	10.83318766	-229.50854304	-112.52497971	-93.19299193
0.08	693.58382905	-339.09351077	-563.26052756	-138.50069745	-148.12257035
0.09	-436.46371828	993.18829365	-109.49191995	-113.75704664	-254.37738555
0.10	-2023.50160551	286.19686267	-304.47825418	-114.03932614	-374.15217067
$c_{\text{sum}}(\tilde{Y})$	4.5336×10^{1}	4.9407×10^{1}	1.0860×10^{1}	5.9182×10^{-1}	1.0813×10^{0}
Time \ Node	6	7	8	9	10
0.00	-134.42864898	-1.93641164	21.64139003	-1.66147063	-1.84016972
0.01	-39.39506553	-4.62758511	13.65093191	5.37816694	-1.86019476
0.02	65.35188033	-0.28689622	-6.09078192	1.03468455	-1.83432791
0.03	76.52750915	1.24942478	-9.90146478	43.33886443	1.36909524
0.04	73.31240011	1.20654232	-9.48121558	2.97522912	2.35608973
0.05	71.71011823	1.07633725	-9.26780939	-9.84460397	-1.04745268
0.06	71.21360156	1.05675949	-9.33881149	-5.95160973	3.85117199
0.07	71.61921015	1.06765961	-9.41391384	-5.06707205	0.66757478
0.08	72.88968254	1.09664112	-9.46189811	-4.91521667	0.62205186
0.09	74.70064101	1.12792462	-9.49586469	-5.04817118	1.11605124
0.10	77.19313329	1.16720479	-9.47610798	-5.21859942	4.44492347
$c_{\text{sum}}(\tilde{Y})$	7.9448×10^{-2}	4.8848×10^{-2}	8.9607×10^{-4}	2.5896×10^{-4}	2.5217×10^{-6}

Chapter 4

Conclusion

The goal of this thesis was to explore the potential of a system of a chain of pendulums with springs to represent beam behavior. To achieve this, a variational approach was chosen as applicable solvers have been shown to exhibit good long-term behavior. To this end, necessary theory for Hamiltonian systems, including the numerical integration method, RATTLE, was presented.

Comparisons with the widely used Euler-Bernoulli beam (2.1.5) theory have revealed similarities in the structure between the two models, and it has been shown that the same angles are considered. Numerical experiments and simulations have demonstrated the viability of the Chain of Pendulums model for various beam configurations (2.2.3), (2.4.2), (2.4.3), specifically the Cantilever, Fixed-Fixed, and Pinned-Pinned supports. By extending the model further, it has been shown to be able to accomodate non-conservative forces in the dissipative Chain of Pendulums model (2.4.4). As the energy of the system dissipates, the model has been shown to converge to static configurations, further validating the model.

To explore and represent the behavior of the model with control forces, we focused on the example of the marine riser. Specifically, we considered the effects external forces have on the bending moment at the origin. Control forces were introduced and their effects on the system were investigated, demonstrating the feasibility of the model to be used to obtain control forces that counteract the external forces and thus reduce the bending moment.

Additionally, the ability to lock and unlock the position of the final node has been explored, offering alternative ways of minimizing bending moments that potentially reduce the necessary control force and energy consumption.

Furthermore, optimal control was considered. Local solvers were utilized due to computational complexity. Although the solution space presented challenges with numerous local minima, the relationship between the control forces and objective function was observed to be convex. A gradient-based stepping approach was implemented as a result. Two objective functions were considered, the bending moment in the final time step, and the bending moment in every time step. Optimization was performed for both constant and variable force cases.

Due to the limited timeframe of the simulations, the optimal control forces were found to be significantly higher than the external forces and often applied in the same direction. This phenomenon was attributed to a proportional backward propagating wave induced by the control forces. Additionally, as the highest bending moment was obtained in the final time step, the optimal control forces of the two objective functions were similar.

In the case of the variable control, the relationship between the objective function and control forces was found to be nonconvex. However, despite this, the method was still effective in finding solutions that were lower than those in the constant control case. This indicates the benefits of a variable control. While the search for global optima in the variable control case is left for future work, it is evident that the Chain of Pendulums model offers a feasible approach for modeling beams with various supports affected by transverse forces. Furthermore, it has been shown to be a useful tool to obtain control forces that result in desired configurations through optimal control.

Bibliography

[1] Ruschel A et al. 'Wellhead fatigue analysis considering the effect of wind-sea and swell waves by using Univariate Dimension Reduction Method'. In: *Journal of Petroleum Science and Engineering* 206 (2021), p. 108989.

[2] Gustad HS. 'Bruk av kunstige nevrale nettverk til å predikere bøyemomenter til stigerør'. MA thesis. NTNU, 2019.

[3] Yadav P, Kumar R, Panda SK, Chang C. 'Energy-efficient thrust allocation for semi-submersible oil rig platforms using improved harmony search algorithm'. In: *IEEE Transactions on Industrial Informatics* 8.4 (2012), pp. 913–924.

[4] Hairer E, Hochbruck M, Iserles A, Lubich C. 'Geometric numerical integration'. In: *Oberwolfach Reports* 3.1 (2006), pp. 805–882.

[5] Duque D. 'A derivation of the beam equation'. In: *European Journal of Physics* 37.1 (2015), p. 015002.

[6] Armero F, Romero I. 'On the formulation of high-frequency dissipative time-stepping algorithms for nonlinear dynamics. Part I: low-order methods for two model problems and nonlinear elastodynamics'. In: *Computer Methods in Applied Mechanics and Engineering* 190.20-21 (2001), pp. 2603–2649.

[7] Bloch A, Brogliato B. 'Nonholonomic mechanics and control'. In: *Appl. Mech. Rev.* 57.1 (2004), B3–B3.

[8] Lee T, Leok M, McClamroch NH. 'Global formulations of Lagrangian and Hamiltonian dynamics on manifolds'. In: *Springer* 13 (2017), p. 31.

[9] Bauchau OA, Craig JI. 'Euler-Bernoulli beam theory'. In: *Structural analysis*. Springer, 2009, pp. 173–221.

[10] Ge SS, Zhang S, He W. 'Modeling and control of an Euler-Bernoulli beam under unknown spatiotemporally varying disturbance'. In: *Proceedings of the 2011 American Control Conference*. IEEE. 2011, pp. 2988–2993.

[11] How B, Ge S, Choo Y. 'Active control of flexible marine risers'. In: *Journal of Sound and Vibration* 320.4-5 (2009), pp. 758–776.

[12] Hong KS, Shah UH. 'Vortex-induced vibrations and control of marine risers: A review'. In: *Ocean Engineering* 152 (2018), pp. 300–315.

[13] Arnold M, Brüls O, Linn J. 'THREAD - Numerical modelling of highly flexible structures for industrial applications'. In: *Mathematics with industry: driving innovation, Annual Report 2019*. ECMI. 2019, pp. 20–25.

[14] Bauchau OA et al. 'Validation of flexible multibody dynamics beam formulations using benchmark problems'. In: *Multibody system dynamics* 37 (2016), pp. 29–48.

[15] Valembois R, Fisette P, Samin JC. 'Comparison of various techniques for modelling flexible beams in multibody dynamics'. In: *Nonlinear Dynamics* 12 (1997), pp. 367–397.

[16] Betsch P, Steinmann P. 'A DAE approach to flexible multibody dynamics'. In: *Multibody system dynamics* 8 (2002), pp. 365–389.

[17] Öchsner A. *Classical beam theories of structural mechanics*. Vol. 42. Springer, 2021.

[18] Sahin A. 'Matrix Method Development for Structural Analysis of Euler Bernoulli Beams with Finite Difference Method'. In: *Afyon Kocatepe Üniversitesi Fen Ve Mühendislik Bilimleri Dergisi* 16.3 (2016), pp. 693–710.

[19] Rajan SD. *Introduction to Structural Analysis & Design*. John Wiley & Sons, 2000.

[20] Marsden JE, West M. 'Discrete mechanics and variational integrators'. In: *Acta numerica* 10 (2001), pp. 357–514.

[21] Pilkey WD, Pilkey WD. *Formulas for stress, strain, and structural matrices*. Vol. 107. John Wiley & Sons Hoboken, NJ, USA, 2005.

[22] Kirk DE. *Optimal control theory: an introduction*. Courier Corporation, 2004.

[23] Lewis FL, Vrabie D, Syrmos VL. *Optimal control*. John Wiley & Sons, 2012.

[24] Timoshenko S. *Strength of materials*. 1930.

[25] Boggs PT, Tolle JW. 'Sequential quadratic programming for large-scale nonlinear optimization'. In: *Journal of computational and applied mathematics* 124.1-2 (2000), pp. 123–137.

[26] Kraft D. 'A software package for sequential quadratic programming'. In: *Forschungsbericht-Deutsche Forschungs- und Versuchsanstalt fur Luft- und Raumfahrt* (1988).

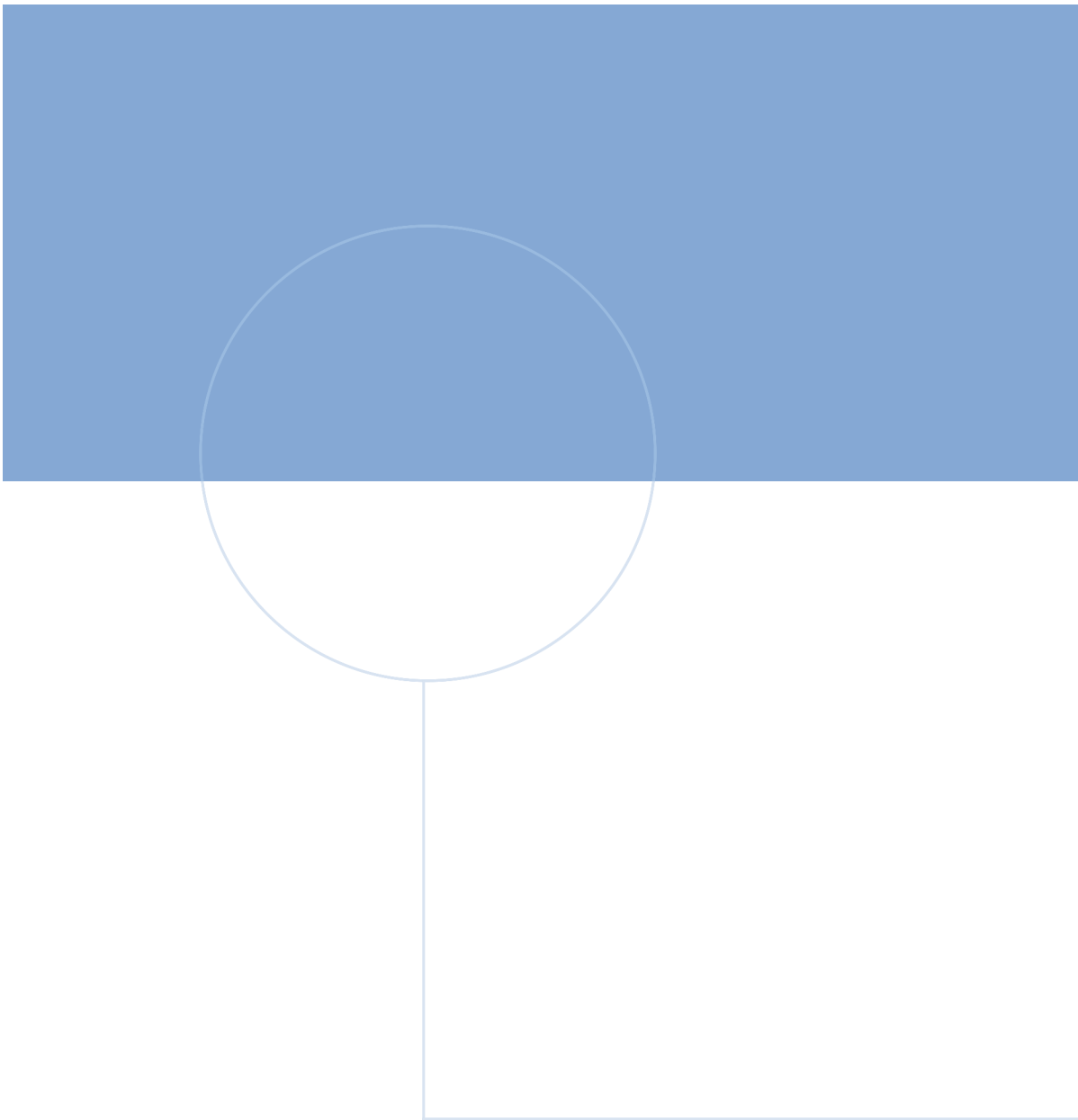

NTNU

Norwegian University of
Science and Technology